MASTERS THESIS

Modeling and Boundary Observer design of Two Phase CO2 Heat Exchanger

Author:
Mohammad GHOUSEIN

Supervisor:
Emmanuel WITRANT

A thesis submitted in fulfillment of the requirements for the degree of Masters in Automatic Control

in the

GIPSA-Lab
Control Department

July 5, 2017

Declaration of Authorship

I, Mohammad GHOUSEIN, declare that this thesis titled, "Modeling and Boundary Observer design of Two Phase CO2 Heat Exchanger" and the work presented in it are my own. I confirm that:

- This work was done wholly or mainly while in candidature at GIPSA-Lab and with Collaboration with CERN Switzerland for Experimental Validation.
- Where any part of this thesis has previously been submitted for a degree or any other qualification at any other institution or University, this has been clearly stated.
- Where I have consulted the published work of others, this is always clearly attributed.
- Where I have quoted from the work of others, the source is always given. With the exception of such quotations, this thesis is entirely my own work.
- I have acknowledged all main sources of help.
- Where the thesis is based on work done by myself jointly with others, I have made clear exactly what was done by others and what I have contributed myself.

Signed:

Date:

Abstract

Mohammad GHOUSEIN

Modeling and Boundary Observer design of Two Phase CO2 Heat Exchanger

In this work, we consider estimation of the thermodynamic properties (Pressure, Enthalpy, Temperature) and mass flow rates along the pipes of a concentric heat exchanger tube in which we have CO_2 as the working refrigerant. The transport phenomena is modeled using Navier-Stokes equations in 1D for both hot and cold sides, where we consider single and two phase flows. The estimation is done with a PDE observer that uses measurements taken at the tube boundaries to construct the required profiles along the tubes. The convergence of this observer is proved using Lyapunov analysis, then the simulation results are validated experimentally on the refrigeration test apparatus built in CERN Switzerland.

Key words: Boundary Observers, Boundary Control, Hyperbolic partial differential equations, fluid dynamics, Equations of State(CO2), Numerical Simulation Methods

Acknowledgements

I would like to express my deepest appreciation to all those who provided me the possibility to complete this report. Starting with all my professors in the MiSCIT master who gave me all the important knowledge in control theory and especially my supervisor Emmanuel WITRANT, for his wise and experienced guidance during the whole time of this internship.

Also, a very big thank you to the colleagues working in CERN, Paolo PETAGNE, Benjamin BRADU and Viren BAHNOT for all the advises and for supervising the experimental tests to validate my work.

In addition, for my professors in the Lebanese University, I would like to say thank you because you gave me all the necessary scientific background in mathematics, physics, electrical engineering and control engineering during the whole past 4 years.

Note:
"This work has been partially supported by the LabEx PERSYVAL-Lab (ANR-11-LABX-0025-01) funded by the French program Investissement d'avenir".

Contents

List of Figures

General Introduction

Heat Exchangers are widely used in many industrial domains like food production, chemical plants, oil refineries and they also represent an important tool for cooling and heating of houses , companies, cars,.. etc. An extensive study on the control of such units is thus vital in order to have lower rates of energy consumption while maximizing the heat transfer rates. In the past decades, fluorocarbons(C_2F_6, C_3F_8,$R134a$) were used as the working fluids for heat exchangers, but nowadays CO_2 cooling has become an interesting technology due to the several advantages that CO_2 has over other fluids. CO_2 has high heat transfer capabilities , high latent heat, low pressure drop, low viscosity (ability to use small size pipes), this allows a network of long small piping over large distances and then it's the best choice for HEP detectors cooling in CERN [20]. The above important facts motivate our work, to model and build estimation techniques for heat exchanger plants that use CO_2 as its working fluid.

Consequently, we consider a long concentric tube pipe as our system in which (two phase -single phase) or (single phase-single phase) carbon dioxide exchange heat through the wall interface. In Chapter 1, the state of the art for the whole work is presented starting with various models found in the literature for modeling of single and two phase flows (3D models,Two fluid models, Homogeneous Equilibrium models). In Chapter 2, the chosen model is established with the necessary assumptions, an approximation of the Equation of state (EoS) is also discussed with the numerical scheme used in the simulations, then the simulation results are shown and discussed. In Chapter 3, the boundary observer is built by linearizing the system to take advantage of linear and quasi-linear hyperbolic systems studied in the literature, then the observer is built on these linearized dynamics.In addition, the estimation error exponential convergence is proved using Lyapunov analysis techniques and confirmed by simulations. In Chapter 4, the actual plant is presented with the tests done at CERN and our results are compared against the experimental data. The designed observer captures the dynamics of the real plant with correction of the modeling errors starting from different initial conditions. In Chapter 5, our conclusion on the work is given with the perspectives and future work.

Chapter 1

The state of the Art

1.1 Introduction

Two phase flow is a flow of vapor and liquid usually inside a tube. It can take various forms and configurations. The aim of this chapter is to discuss the types of two phase flow regimes, as well as the general way of physical modeling used to deal with such systems.

1.2 Physical Modeling

In this section, we first address the behavior of a fluid moving in a horizontal tube with a phase change, which means that we have a combination of liquid and vapor at the same time inside the tube. As shown in Fig (1.1), different flow regimes can be divided into two groups: (a) those in which vapor flows as a continuous stream, and (b) those in which vapor segments are separated from each other by liquid. The time averaged fraction of the tube that is occupied by vapor is the void fraction α. From experiments, it is observed that vapor flows continuously for $\alpha > 0.5$. At high void fraction and low vapor flow rate, the liquid is smooth and stratified. As we increase the vapor flow rate, waves appear on the liquid-vapor interface, continue increasing will lead the liquid to climb up the tube wall and the flow is (annular). At high vapor flow rate, the liquid is still on the walls but some liquid droplets are entrained in the vapor flow and this flow is (annular-mist flow). At low void fraction $\alpha < 0.5$, the continuity is broken (Slug flow), in this type of flow the slug moves faster than the liquid. At lower void fractions, the vapor is contained in the liquid in the form of elongated bubbles (Plug flow). Further decreasing the void induces the (bubbly flow): in this regime the interface between the liquid and vapor is not significant, bubbles and liquid flow at approximately the same speed.

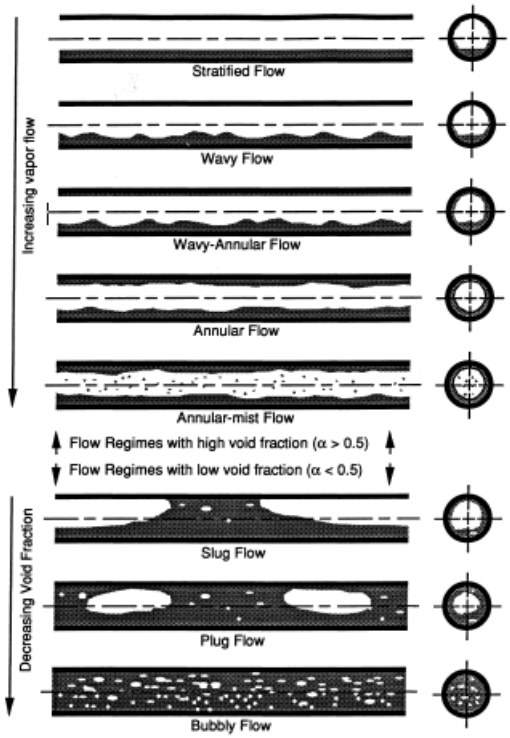

FIGURE 1.1: Vapor-liquid flow regimes [8]

1.2.1 3D Two Fluid Model

As described above, different flow regimes have their own characteristics which seek a general way of modeling. The basic modeling strategy found in the literature is to consider a control volume in which liquid and vapor are separated by an interface, through this interface mass, momentum, heat and volume exchange occurs : this is the so called "Two fluid Models". The derivation of the most general equations in which there is variations in (x,y,z,t) and non-thermodynamic equilibrium between the phases (i.e mass, momentum, heat and volume exchange don't happen instantaneously, there is some time for the transition) comes from the basic laws of physics: conservation of mass, conservation of momentum (Newton's second law), conservation of energy (1st law of thermodynamics) and the 2nd law of thermodynamics (Entropy never decrease). At this step in modeling we consider only continuum assumptions and all our state variables are well defined. The derivation is done in [21] [14], for the multi-phase case and the results are given by:

Conservation of mass

$$\frac{\partial \rho_k}{\partial t} + \nabla.(\rho_k v_k) = 0 \tag{1.1}$$

Conservation of momentum

$$\frac{\partial (\rho_k v_k)}{\partial t} + \nabla.(\rho_k v_k \otimes v_k) = (-\nabla.p_k + \nabla.\tau_k + \rho_k b_k) \tag{1.2}$$

Conservation of Energy

$$\frac{\partial (\rho_k (e_k + \frac{1}{2} v_k^2))}{\partial t} + \nabla.(\rho_k (e_k + \frac{1}{2} v_k^2)) = \nabla.((\tau_k - p_k I).v_k - q_k) + \rho_k (r_k + b_k.v_k) \tag{1.3}$$

Where k = g (gas, vapor) or k = l (liquid)

ρ_k : density of each phase	v_k : velocity of each phase
p_k : pressure of each phase	τ_k : stress tensor on each phase
e_k : Internal energy of each phase	q_k : heat transfer between the the phases
r_k : External heat source	b_k : Body forces on each phase (gravity for example)

In [14] the author proved that energy transport is equivalent to the entropy transport. These entropy relations are used by several authors to derive relaxation terms as we will see later.

Equations (1.1) - (1.3) are bulk equations for the phases, but in multi-phase flow, phases interact with each other through an interface. The assumptions made that the we consider the interface has no mass, then it has no momentum and no kinetic energy but it has internal energy. By taking a control volume attached to the interface and also applying the basic laws of physics we get:

Interface Relations

Mass relation: Mass entering interface = Mass leaving the interface:

$$\rho_g(v_g - vi).n_g + \rho_l(v_l - vi).n_l = 0 \tag{1.4}$$

Momentum relation: Here we notice the appearance of the surface tension with its two components: the tangential one (caused by curvature of the interface) and normal one (caused by temperature gradients). Applying the sum of forces on the interface we get:

$$0 = \rho_g v_g \otimes (v_g - v_i).n_g + \rho_l v_l \otimes (v_l - v_i).n_l - (\tau_g - p_g I).n_g - (\tau_l - p_l I).n_l - \nabla_s \sigma - 2\sigma H_{s,g} \tag{1.5}$$

Energy relation: The interface has internal energy but no kinetic energy, hence the variation of the internal energy inside the interface is given by:

$$\begin{aligned}\frac{\partial(e_s)}{\partial t} + \nabla_s.(v_i e_s) = -\rho_g(e_g + \frac{1}{2}v_g^2)(v_g - vi).n_g - \rho_l(e_l + \frac{1}{2}v_l^2)(v_l - vi).n_l + (\tau_g - p_g I).v_g.n_g \\ +(\tau_l - p_l I).v_l.n_l - q_g n_g - q_l n_l + r_s + 2\sigma H_{s,g}.n_g.v_i + v_i.\nabla_s \sigma\end{aligned} \tag{1.6}$$

where:

- v_i: Interface velocity
- n_g, n_l : Unit normal to the interface in direction outwards of phase g and l respectively
- σ : Surface tension
- $H_{s,g}$: Algebraic value of the minimum curvature of the interface
- e_s : Internal energy of the interface
- r_s : Heat by the source varying the internal energy of the interface

Equations (1.1) - (1.3) and (1.4) - (1.6) are the basic equations for the two phase modeling. It is noticed that the dimension of the system is very large: we have variations in (x,y,z,t) and interface relations where we have a lot of unknowns. Then to reduce complexity, averaging techniques are applied.

1.2.2 Averaging and The 1D Two Fluid Model

There exists various types of averaging. Spatial averaging consists of averaging the physical quantities over a given domain (like cross-section of the tube in our case) [21] i.e instead of having variations in (x,y,z,t), if we average along the cross-section we have variation in (x,t)). Time averaging consists in looking at a given point in space and averaging the quantities over time. Ensemble averaging consists of averaging the quantities at a given time and at a given location taking into account all the possible realizations of the flow [14]. Averaging always implies a lose of information on the flow but in some applications we are not concerned on knowing every detail of the flow in (x,y,z,t), so averaging may reduce the complexity of the equations. To take into account the tube cross-section, we use area averaging as most of the literature on the 1D model. For the interface, and considering non-equilibrium models (different pressure, temperature, velocities, chemical potentials between the phases), the interface exchange (mass,momentum,heat and volume) are modeled by relaxation terms.

Some useful definitions:

- *Relaxation time:* time needed by the system to go into equilibrium after being perturbed.
- *Chemical potential:* form of potential energy that can be absorbed or released during a chemical reaction or phase change.

In the 1D two fluid model, the two phases are assumed to have **separate pressures P_k, temperatures T_k, chemical potentials μ_k and velocities** v_k. The system can be moved towards equilibrium by employing relaxation terms. The model equations are given by:

Mass Conservation

$$\frac{\partial(\alpha_g\rho_g)}{\partial t}+\frac{\partial(\alpha_g\rho_g v_g)}{\partial x}=K(\mu_l-\mu g) \tag{1.7}$$

$$\frac{\partial(\alpha_l\rho_l)}{\partial t}+\frac{\partial(\alpha_l\rho_l v_l)}{\partial x}=K(\mu_g-\mu l) \tag{1.8}$$

Momentum Conservation

$$\frac{\partial(\rho_g\alpha_g v_g)}{\partial t}+\frac{\partial(\rho_g\alpha_g v_g^2)}{\partial x}+\alpha_g\frac{\partial P_g}{\partial x}+\Delta P_{ig}\frac{\partial\alpha_g}{\partial x}+F(v_g-v_l)=\rho_g\alpha_g g_x+f_{w,g}+v_iK(\mu_l-\mu g) \tag{1.9}$$

$$\frac{\partial(\rho_l\alpha_l v_l)}{\partial t}+\frac{\partial(\rho_l\alpha_l v_l^2)}{\partial x}+\alpha_l\frac{\partial P_l}{\partial x}+\Delta P_{il}\frac{\partial\alpha_l}{\partial x}-F(v_g-v_l)=\rho_l\alpha_l g_x+f_{w,l}-v_iK(\mu_l-\mu g) \tag{1.10}$$

Energy Conservation

$$\begin{aligned}\frac{\partial(\rho_g\alpha_g H_g-\alpha_g P_g)}{\partial t}+\frac{\partial(\rho_g\alpha_g v_g H_g)}{\partial x}+P_iv_i\frac{\partial\alpha_g}{\partial x}&=\rho_g\alpha_g v_g g_x+Q_{w,g}-H(T_g-T_l)\\&\quad -P_iJ(P_g-P_l)+v_iF(v_l-v_g)+E_{g,i}K(\mu_l-\mu g)\end{aligned} \tag{1.11}$$

$$\begin{aligned}\frac{\partial(\rho_l\alpha_l H_l-\alpha_l P_l)}{\partial t}+\frac{\partial(\rho_l\alpha_l v_l H_l)}{\partial x}+P_iv_i\frac{\partial\alpha_l}{\partial x}&=\rho_l\alpha_l v_l g_x+Q_{w,l}+H(T_g-T_l)\\&\quad +P_iJ(P_g-P_l)-v_iF(v_l-v_g)-E_{g,i}K(\mu_l-\mu g)\end{aligned} \tag{1.12}$$

Pressure Relaxation

$$\frac{\partial\alpha_g}{\partial t}+v_i\frac{\partial\alpha_g}{\partial x}=J(P_g-P_l) \tag{1.13}$$

where k = g (gas, vapor) or k = l (liquid)

- H_k : total Enthalpy ($H_k = h_k + \frac{1}{2}v_k^2$) and h_k : specific enthalpy
- $Q_{w,k}$: heat transfer from the wall to the phase k
- α_k : void fraction of the phase k
- $f_{w,k}$: friction done by the wall
- g_x: projection of the gravitational acceleration on the tube axis
- H, J, F, K: relaxation constants
- P_i: interface pressure and $\Delta P_{ik} = P_k - P_i$
- $E_{g,i} = \mu^* + \frac{1}{2}v_i^2$ and μ^* is the effective interface chemical potential.

In addition it's necessary for the second law of thermodynamics to be satisfied. If we neglect the velocity relaxation, it was proved by [9] that the second law will be obeyed if:

- $H \geq 0$
- $J \geq 0$
- $K \geq 0$
- $min(P_g, P_l) \leq P_i \leq max(P_g, P_l)$
- $min(\mu_g, \mu_l) \leq \mu^* \leq max(\mu_g, \mu_l)$

Note that ΔP_{ik} in the momentum equations is the correction pressure term, which plays an important role in the model hyperbolicity because in the absence of this term the model becomes non hyperbolic, which leads to a lack of existence of a stable mathematical model as well as a loss of the stability of numerical methods [16].

This hyperbolicity condition [16] is satisfied (neglecting pressure relaxation) if we take:

$$\Delta P = \delta \frac{\alpha_g \alpha_l \rho_g \rho_l}{\rho_g \alpha_g + \rho_l \alpha_l} (v_g - vl)^2 \tag{1.14}$$

with $\delta = 0.2$.

In addition, the velocity of the interface can be taken as the average value:

$$v_i = \alpha_g v_g + \alpha_l v_l \tag{1.15}$$

This general model is found and studied by many authors with slight differences on the assumptions. For example, [13] studies the effect of all relaxation terms neglecting the velocity,[15] provides a numerical study considerenig pressure and velocity relaxation, [4] models CO_2 depressurization pipelines and also [19] uses this model in studying the transition in metastable liquids. In addition, [2] present this general model in presenting CO_2 transportation along pipelines.

1.2.3 Homogenous Equilbrium Model

This model is the most simplified form that can be obtained from the above two fluid model, wherein the two phases are assumed to travel together at the same velocity and behave as single phase with properties that are defined as a weighted average of the properties of the individual phases. First the following assumptions are taken:

- No relative motion between the phases ($v = v_g = v_l$))
- Phase change, transfer of volume, heat transfer between the phases happen instantaneously (i.e we have thermodynamic equilibrium ($P = P_g = P_l, T = T_g = T_l, \mu = \mu_g = \mu_l$)
- Body forces are neglected (gravity)

Then the model equations can be written as follows:

Mass Conservation

$$\frac{\partial \rho}{\partial t} + \frac{\partial (\rho v)}{\partial x} = 0 \tag{1.16}$$

Momentum Conservation

$$\frac{\partial (\rho v)}{\partial t} + \frac{\partial (\rho v^2 + P)}{\partial x} = f_w \tag{1.17}$$

Energy Conservation

$$\frac{\partial (\rho H - P)}{\partial t} + \frac{\partial (\rho v H)}{\partial x} = Q_{ext} \tag{1.18}$$

where:

- ρ : Average density of the mixture ($\rho = \alpha_g \rho_g + \alpha_l \rho_l$)
- v: Fluid velocity
- P: Pressure of the system
- H: Total Enthalpy ($H = h + \frac{1}{2} v^2$)
- Q_{ext}: External Heat Source
- f_w : Wall friction

The model is completed by an equation of state as density, pressure and enthalpy are thermodynamically related (for instance, $\rho = f(P, h)$): this relation is discussed in details in the coming chapters.

1.3 Conclusion

In this chapter we have seen several two phase models, these models emerges from the fundamental laws of physics. We seek a control oriented model that can capture the necessary dynamics of the system so that we can design our boundary observer based on it. In the next chapter, the modeling phase is extensively explained with all the assumptions taken and numerical simulations done.

Chapter 2

Problem Formulation and Model Implementation

2.1 Introduction

The aim of this chapter is to describe the heat exchanger considered and the transport equations used in modeling. The model is prepared for simulation by discussing the approximation of the Equation of State (EoS) for CO_2 in the two and single phase regions as well as the numerical scheme used in the implementation. At the end, the simulation results are presented and discussed.

2.2 Problem formulation

We are interested in building boundary observation techniques capable of estimating distributed thermodynamic profiles from boundary measurements for a concentric tube heat exchanger found in *CERN, Switzerland*. The basic idea of heat exchangers is that we have two fluids (hot and cold) and they are exchanging heat through an interface (wall).

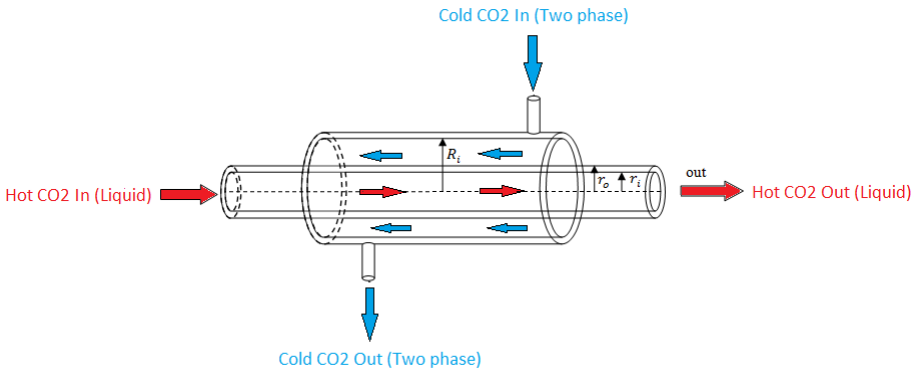

FIGURE 2.1: CO_2 Two phase heat exchanger (Evaporator)

As shown in Fig (2.1), on the hot side CO_2 enters in liquid state and remains liquid at the outlet. On the cold side, CO_2 enters in a two-phase state and leaves in two-phase. The interesting thing in this system is the change of phase behavior inside the outer tube, which makes the detailed modeling more complicated as the liquid is changing into vapor as it flows into the exchanger.

2.2.1 Model Equations

Besides the complexity in dealing with two-phase flows as seen in Chapter 1 (two fluid model equations), CO_2 has a very important characteristics: **the ratio of liquid density to vapor density (ρ_l/ρ_v) is small [18], this results in more homogeneous two phase flows**. It's reasonable to assume that liquid and vapor phases are mixed and propagate at the same velocity, this will decrease the complexity of modeling the two phase side. As a result the following assumptions are taken:

- Homogenous flow for both liquid and two phase fluids
- Neglect kinetic and potential energies
- Neglect wall thickness and assume overall heat transfer coefficient
- Heat exchanger is in a vacuum insulation from the outside

Then using the Homogenous Equilbrium model (1.16)-(1.18), the model equations are as follows:

Cold fluid (Two phase)

Mass Conservation

$$A_c\frac{\partial \rho_c}{\partial t} - \frac{\partial \dot{m}_c}{\partial x} = 0 \tag{2.1}$$

Momentum Conservation

$$\frac{\partial \dot{m}_c}{\partial t} - \frac{\partial}{\partial x}(\frac{\dot{m_c}^2}{\rho_c A_c}) - A_c\frac{\partial P_c}{\partial x} + \frac{f_2 \dot{m}_c|\dot{m_c}|}{2D_H\rho_c A_c} = 0 \tag{2.2}$$

Energy Conservation

$$A_c\frac{\partial(\rho_c H_c - P_c)}{\partial t} - \frac{\partial(\dot{m}_c H_c)}{\partial x} = \pi D_1 \alpha (T^H - T^C) \tag{2.3}$$

Hot fluid (Single phase)

Mass Conservation

$$A_H\frac{\partial \rho_H}{\partial t} + \frac{\partial \dot{m_H}}{\partial x} = 0 \tag{2.4}$$

Momentum Conservation

$$\frac{\partial \dot{m_H}}{\partial t} + \frac{\partial}{\partial x}(\frac{\dot{m_H}^2}{\rho_H A_H}) + A_H\frac{\partial P_H}{\partial x} + \frac{f_1 \dot{m_H}|\dot{m_H}|}{2D_1\rho_H A_H} = 0 \tag{2.5}$$

Energy Conservation

$$A_H\frac{\partial(\rho_H H_H - P_H)}{\partial t} + \frac{\partial(\dot{m_H} H_H)}{\partial x} = -\pi D_1 \alpha (T^H - T^C) \tag{2.6}$$

with k = C (cold fluid) , k = H (hot fluid):

ρ_k : density (Kg/m^3)
P_k : pressure (Pa)
H_k : specific enthalpy (J/kg)
$\dot{m}_k$: mass flow rate (Kg/s)
T^k : temperature (K)
α : overall heat transfer coefficient $(W/m^2.K)$
A_H, A_c : inner and outer tubes cross-sectional area (m^2)

D_1, D_2, D_H : inner, outer, hydraulic tube diameter respectively (m)
f_k : friction coefficient

Remarks:

- the hot fluid is assumed to be propagating in the +ve x-axis direction and cold fluid in the -ve x-axis direction.
- since CO_2 has a very low viscosity it's natural for our model equations to be like the Euler equations for invicisd flow, adding the heat exchange term between the two fluids.

2.3 Equation of State (EOS)

Most vapor compression cycles are studied on a pressure-enthalpy diagram (P-h diagram) presented in Fig(2.2).

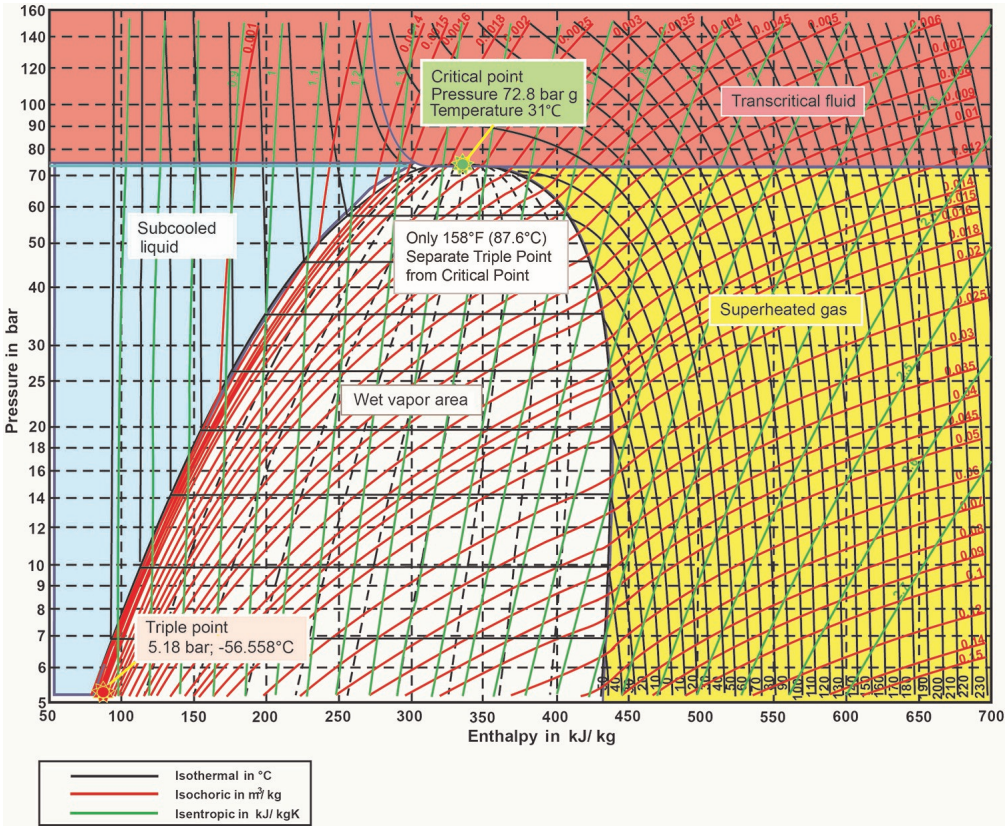

FIGURE 2.2: CO_2 Pressure-Enthalpy Diagram

Choosing P and h as our states, all thermodynamic properties can be calculated. The above equations (2.1)-(2.6) involve density and temperature: these properties and all there necessary partial derivatives are calculated from an equation called the equation of state (i.e $\rho = \rho(P, h)$, $T = T(P, h)$). This equation changes from one region to the other (i.e the equation in the liquid region is different from the two phase region). We choose a range of pressures $(2MPa - 3MPa)$, which is almost the range used in CERN, to deal with two phase flows and our objective is to calculate ρ, T, $\frac{\partial \rho}{\partial P}$, $\frac{\partial \rho}{\partial h}$ in each region.

2.3.1 Two phase region

The properties at the saturation line (T^{sat}, ρ_v^{sat}, ρ_l^{sat}, h_l^{sat},h_v^{sat}) and all the necessary partial derivatives are calculated (for the range of pressures stated above) using Coolprop library [3] and fitted by polynomials of degree 5 in Matlab.

$T = T^{sat}(p)$(Temperature only depends on pressure)	$x = \frac{h-h_l^{sat}}{h_v^{sat}-h_l^{sat}}$ (Quality)
$\alpha = \frac{1}{1-\frac{(h-h_v^{sat})\rho_v^{sat}}{(h-h_l^{sat})\rho_l^{sat}}}$ (Void Fraction)	$\rho = \alpha\rho_v^{sat} + (1-\alpha)\rho_l^{sat}$(Density)
$\frac{\partial\rho}{\partial h} = -\frac{\rho^2}{T^{sat}}\frac{dT^{sat}}{dp}$(Clausius-Clapeyron Equation)	$\frac{\partial\rho}{\partial p} = \frac{\partial}{\partial p}(\alpha\rho_v^{sat} + (1-\alpha)\rho_l^{sat})$

The errors between the polynomials approximations and the Coolprop values are shown in Fig (2.3). The approximations shown in Fig (2.4) are very accurate with a relative error less than 0.01%. This type of approximation is used because Coolprop library is very slow in Matlab and there is no high level interface for computing thermodynamic partial derivatives in the two phase region.

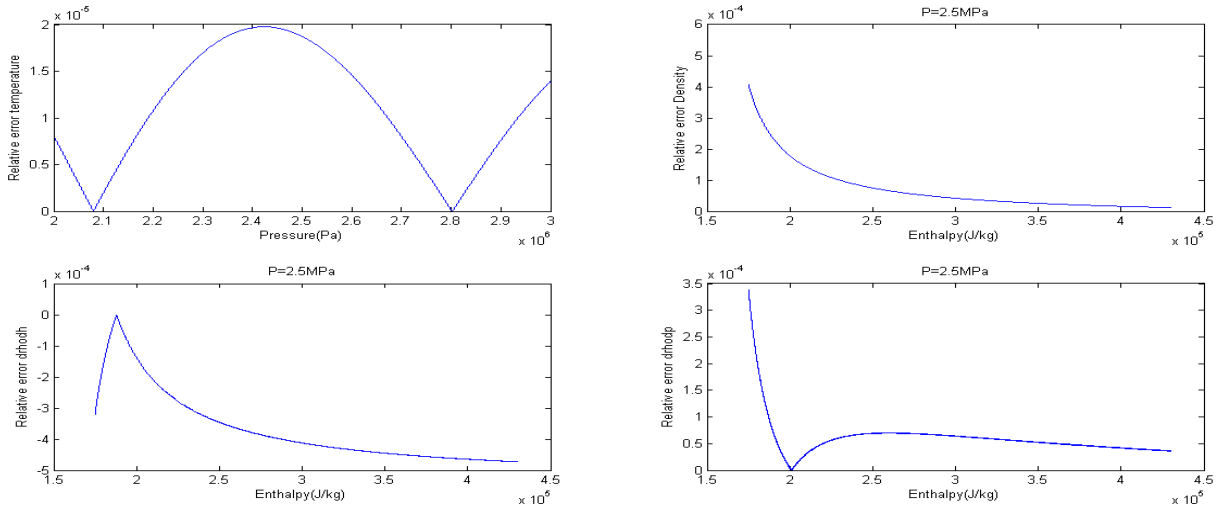

FIGURE 2.3: Relative error: Two Phase Properties

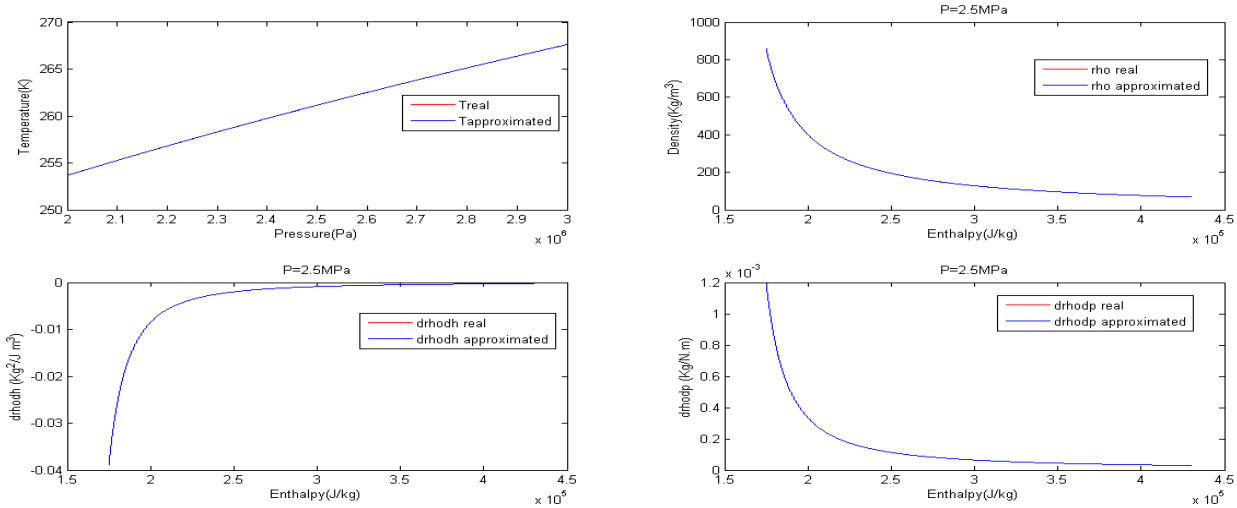

FIGURE 2.4: CO_2 Two Phase Properties

2.3.2 Liquid region

Fig (2.2) shows that in the liquid region, temperature and density almost don't depend on pressure. Taking a point on the saturation curve and making 1st Order Taylor expansion along constant enthalpy lines is thus a good approximation.

First $P^{sat}(h), T^{sat}(h), \rho^{sat}(h), \frac{dT^sat(h)}{dp}, \frac{d\rho^{sat}(h)}{dp}$ where calculated using polynomials of degree 5. Then the properties in the liquid region are calculated as:

$$T(P,h) = T^{sat}(h) + \frac{dT^{sat}}{dp}(P - p^{sat}(h)) \qquad \rho(P,h) = \rho^{sat}(h) + \frac{d\rho^{sat}}{dp}(P - p^{sat}(h))$$

$\frac{\partial \rho}{\partial P}$ and $\frac{\partial \rho}{\partial h}$ are calculated deriving $\rho(P,h)$ with respect to pressure and enthalpy, respectively. These equations are simulated and compared against Coolprop library values. The results are shown in Fig (2.5) and Fig (2.6).

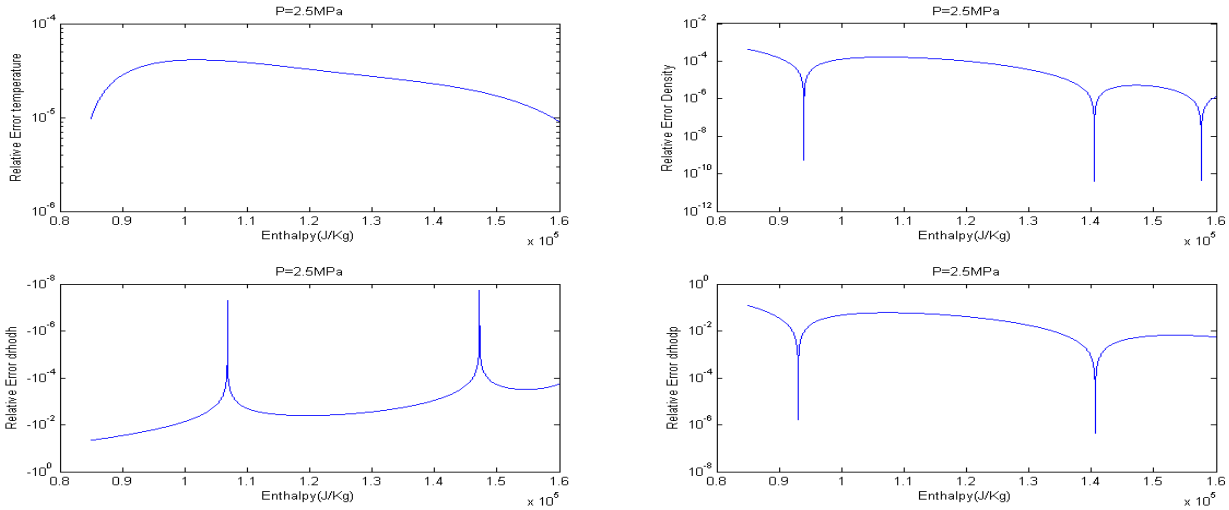

FIGURE 2.5: Relative error: Liquid Region Properties

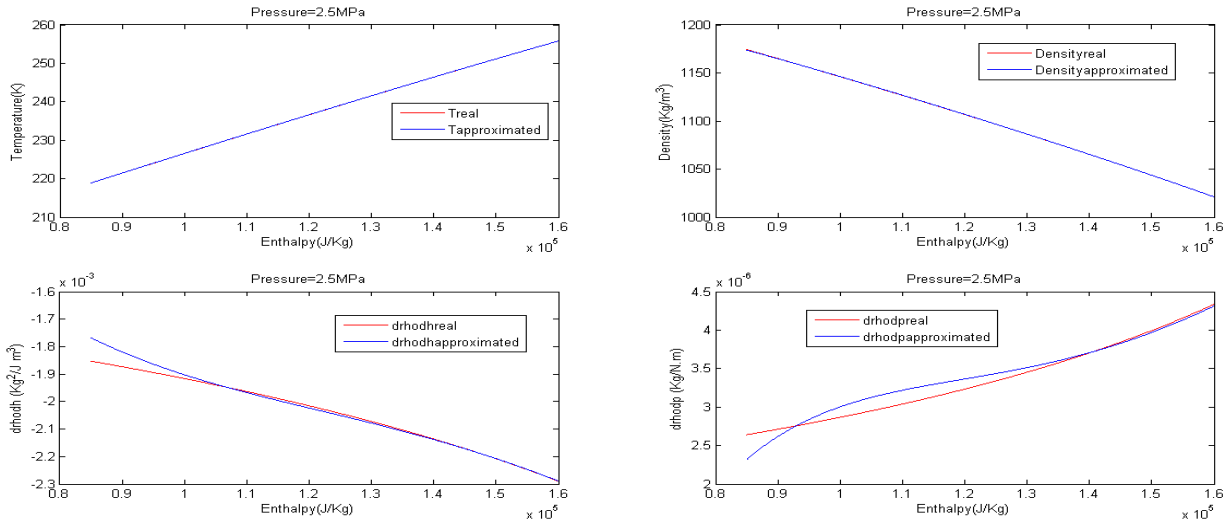

FIGURE 2.6: CO_2 Liquid Properties

The relative error for the liquid region approximation in total is less 10%, which gives us a good approximation as we are using simple Taylor expansion to approximate the complex Equation of State for carbon dioxide.

2.4 Model Implementation

Equations (2.1)-(2.6) were implemented using the Finite Volume Method (FVM). This method consists in dividing the space into a set of control volumes of equal or different sizes and then integrating the conservation equations on each control volume [17]. (FVM) is very efficient when dealing with conservation laws because it's ensured that every conserved quantity (energy ,mass,momentum) is conserved in each control volume. Yet some problems happens when implementing the momentum equations, because in these equation we have a pressure gradient that drives the flow. The authors in [17] argued that implementing the velocity field on the same grid as the pressure field may lead to a nonphysical solution in which we may have certain oscillations called the "Chequerboard Oscillations" and the solution suggested is to implement the momentum equations on a staggered grid mainly for the velocity to be calculated from the difference of pressures between two adjacent cells.

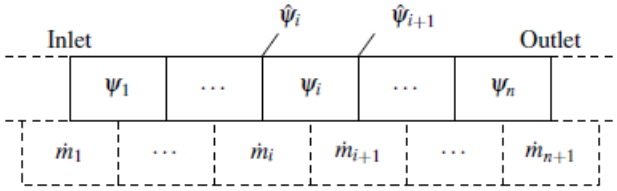

FIGURE 2.7: Finite Volume Grid

As shown in Fig (2.7), we have two grids: the upper grid is for mass and energy equations implementation and the staggered grid is for the momentum equations. ψ_i is the average thermodynamic property in the control volume i (enthalpy,density,pressure..) and $\hat{\psi}$ is the interface value approximated using an upwind scheme as follows:

$$\hat{\psi}_i = (1-\delta_i)\psi_{i-1} + \delta_i\psi_i \qquad and \qquad \delta_i = \begin{cases} 1 & \text{if } \dot{m}_i \leq 0 \\ 0 & \text{if } \dot{m}_i > 0 \end{cases}$$

The equations of the discretized model are written in the section (A.1.1) of the appendix. With the following boundary conditions:

$$\begin{aligned} H_H(0,t) &= H_{in}^H & H_c(L,t) &= H_{in}^C \\ P_H(0,t) &= P_{in}^H & P_c(L,t) &= P_{in}^C \\ \dot{m}_H(L,t) &= \dot{m}_{out}^H & \dot{m}_c(0,t) &= \dot{m}_{out}^C \end{aligned} \tag{2.7}$$

2.5 Simulation results

The simulation results are presented in Fig (2.8),Fig (2.9) and Fig (2.10) using constant boundary conditions and an average values for the heat transfer and friction coefficients.

$H_H(0,t) = 180KJ/Kg$	$H_c(L,t) = 200KJ/Kg$	$P_H(0,t) = 3MPa$	$f_1 = 10$	$f_2 = 15$
$P_c(L,t) = 2.2MPa$	$\dot{m}_H(L,t) = 0.02Kg/s$	$\dot{m}_c(0,t) = 0.02Kg/s$	$nx = 60$	$dt = 0.1s$
$\alpha = 100W/m^2.K$	$L = 17.655m$	$D_1 = 12mm$	$D_2 = 33.4mm$	

Ode15s in Matlab is used to solve the equations because the model is highly stiff .

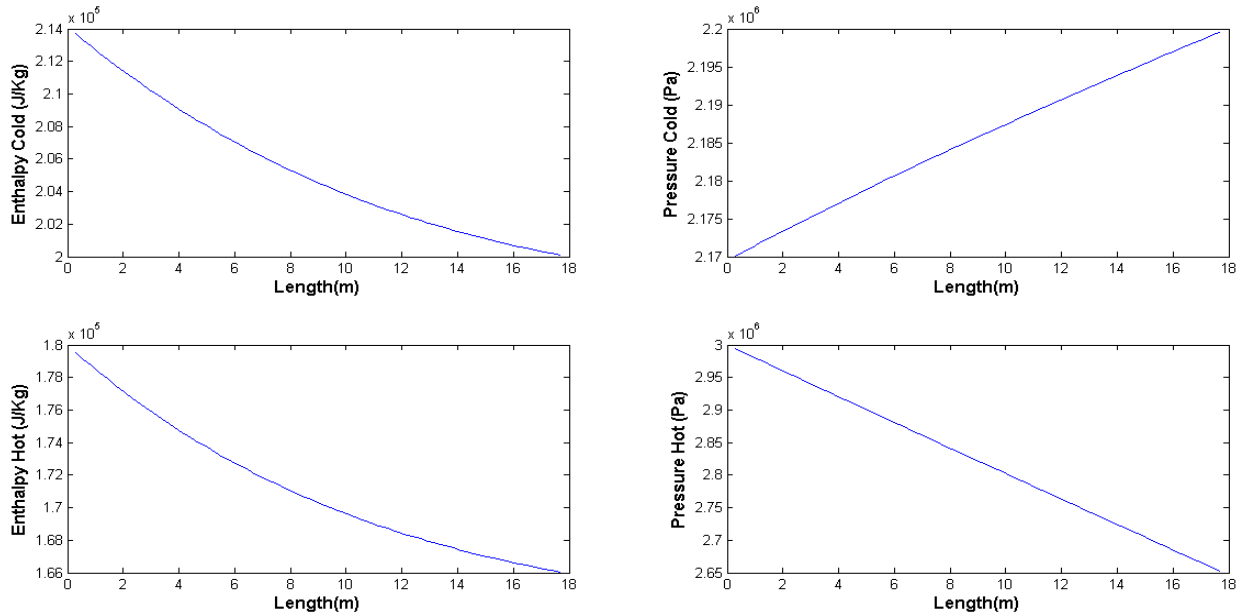

FIGURE 2.8: Steady state: Pressure - Enthalpy

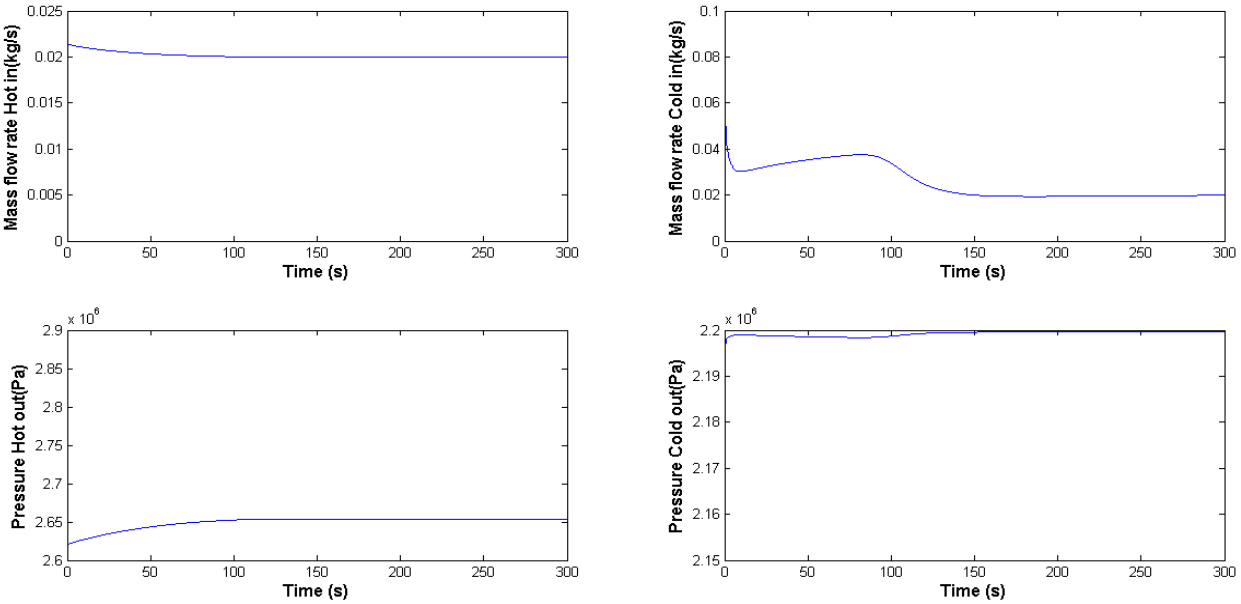

FIGURE 2.9: Pressure - Mass flow rate

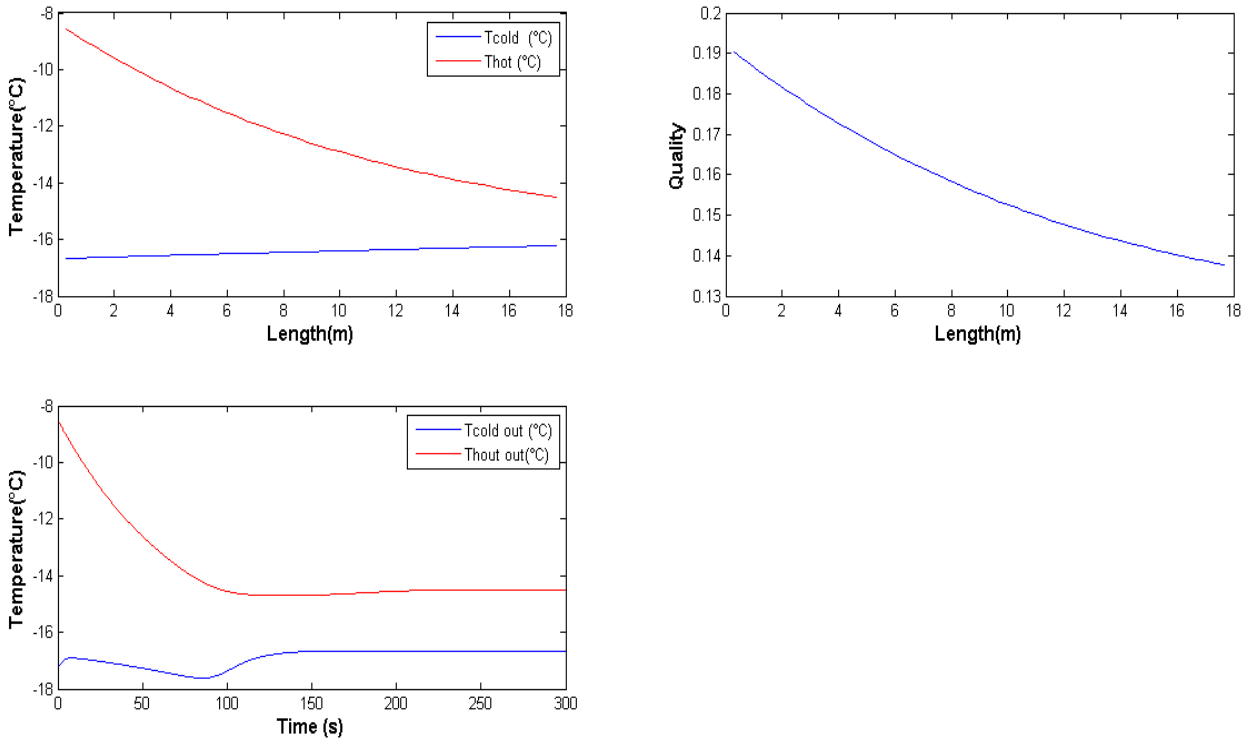

FIGURE 2.10: Quality-Temperature

2.5.1 Discussion

The system is simulated until steady state is reached starting with constant profile initial condition for all the states. At steady state, for the hot side: both enthalpy and temperature decrease with the length since the hot fluid is loosing energy to the cold fluid and this appears in the steady state plots where the hot inlet temperature was ($T_{Hin} = -8.577$ °C) and outlet ($T_{Hout} = -14.5$ °C). For the cold fluid, the cold fluid is gaining energy so its enthalpy should increase in the -ve x-axis direction (cold fluid is flowing from x=L to x=0), since we have two phase flow the temperature should remain constant at the saturation temperature and this is verified as the cold fluid enters at (-16.22 °C) and leaves at (-16.67 °C), which are approximately the same temperatures. The small decreases is due to the pressure drop. The gained energy by the cold fluid increase the quality and this what happens in the steady state quality plot. Regarding pressure drop, the pressure should decrease with the direction of the flow (hot and cold pressure plots). Concerning transient behavior, mass flow rate should be the same along the tube at steady state, this is confirmed by the mass flow plots where the ($\dot{m}_{in} = \dot{m}_{out} = 0.02Kg/s$) for both fluids. The output pressure stabilizes without oscillations and settles into steady state. The same happens for both hot and cold outlet temperatures.

2.6 Conclusion

The model shows a good behavior in simulation conserving the first and second law of thermodynamics. We are reasonably satisfied with the model simulation, and thus use it for the observer design. In the coming chapter, the observer architecture is presented with all the simulation results.

Chapter 3

Observer Design

3.1 Introduction

As we are concerned with estimating the thermodynamic properties of two phase CO_2 fluid flowing in one tube and exchanging heat with another liquid CO_2 flowing in the opposite direction, our system of equations falls in the category of a system of first order hyperbolic nonlinear partial differential equations describing the conservation laws. Hyperbolic systems and especially linear and quasi-linear hyperbolic systems are well studied by the control community due to their wide range of applicability in several domains, the existence of the so called Riemann invariants which is a powerful tool for the proof of classical solutions, analysis and control [1]. These systems are of the following general form:

$$\partial_t \xi(x,t) + \Lambda(x)\partial_x \xi(x,t) = F(x)\xi(x,t) \tag{3.1}$$

where $t \in R^+$ is the time variable, $x \in [0,1]$ is the spatial variable, $\xi : R^+ \times [0,1] \to R^n$, F and Λ are in $C^0([0,1]; \mathcal{R}^{n\times n})$. $\Lambda(x) = diag(\lambda_1..\lambda_n)$ is a diagonal matrix with $\lambda_k < 0$ for $k \in \{1...m\}$ and $\lambda_k > 0$ for $k \in \{m+1,..n\}$.
The above formalization means that we have m waves $\xi_-(x,t)$ propagating from right to left and (n-m) waves $\xi_+(x,t)$ propagating from left to right. Let's also consider the following static boundary condition:

$$\begin{aligned} \xi_-(1,t) &= G_1\xi_-(0,t) \\ \xi_+(0,t) &= G_2\xi_+(0,t) \end{aligned} \tag{3.2}$$

Where G_1 and G_2 are $(m \times m)$ and $(n-m) \times (n-m)$ constant matrices respectively. The problem of controllability and observability for quasilinear hyperbolic systems is considered in [12]. The stability conditions for system (3.1) with boundary conditions (3.2) are proved by [22] using a Lyapunov candidate. The authors in [22] provide stability conditions and propose the reduction of infinite linear matrix inequality (LMI) coming from the Lyapunov analysis to a finite number by using a polytopic approach. The problem of dynamic boundary control stabilization was addressed in [6].

Concerning boundary observers, the idea is less investigated in the literature. The first approach was to discritize the system and then apply basic laws from control theory, but by discritization we may loose some vital information on the dynamics of the system and the observability and controllability depend on the spatial discritization step. Besides, in distributed parameter estimation problems it's impossible to obtain measurements at every position along the domain. It's more natural for sensors to be placed at the boundaries (at the extremities of the tube in our case). In [5] a boundary observer of rightward hyperbolic equations is designed using Lyapunov analysis and

in [23] an infinite-dimensional Luenberger-type observer is proposed using the same Lyapunov candidate used for the exponential stability of one dimensional balance laws in [7].

To take benefit of the theory done on linear and quasilinear systems seen above, linearization is taken as our best choice. As a result the observer is built on these linearized dynamics, as detailed in this chapter.

3.2 Linearization

The system of equations (2.1)-(2.6) is linearized close to the steady state reached by the nonlinear model as follows:

$$\begin{aligned} H_H(x,t) &= H_H^S(x) + \Delta H_H(x,t) & H_c(x,t) &= H_c^S(x) + \Delta H_c(x,t) \\ P_H(x,t) &= P_H^S(x) + \Delta P_H(x,t) & P_c(x,t) &= P_c^S(x) + \Delta P_c(x,t) \\ \dot{m_H}(x,t) &= \dot{m}_{out}^{H,S} + \Delta \dot{m_H}(x,t) & \dot{m_c}(x,t) &= \dot{m}_{out}^{C,S} + \Delta \dot{m_c}(x,t) \end{aligned} \tag{3.3}$$

Using a Taylor expansion of order 1 and given that for each fluid we have a continuously differentiable equation of state $\rho = f(P,H)$ and $T = g(P,H)$ (discussed in Chapter 2) and also considering approximating the non-differentiable function absolute (abs(x)) in the momentum equations by a differentiable function $|x| \approx \sqrt{x^2+\varepsilon}$ for a very small $\varepsilon > 0$, the system is simplified to:

$$A^S(x)\frac{\partial W}{\partial t} + B^S(x)\frac{\partial W}{\partial x} + C^S(x)W = 0 \tag{3.4}$$

where:

$$W = \begin{pmatrix} \Delta \dot{m_H}(x,t) \\ \Delta P_H(x,t) \\ \Delta H_H(x,t) \\ \Delta \dot{m_c}(x,t) \\ \Delta P_c(x,t) \\ \Delta H_c(x,t) \end{pmatrix} \quad A^S(x) = \begin{pmatrix} 0 & a_{12} & a_{13} & 0 & 0 & 0 \\ 1 & 0 & 0 & 0 & 0 & 0 \\ 0 & a_{32} & a_{33} & 0 & 0 & 0 \\ 0 & 0 & 0 & 0 & a_{45} & a_{46} \\ 0 & 0 & 0 & 1 & 0 & 0 \\ 0 & 0 & 0 & 0 & a_{65} & a_{66} \end{pmatrix}$$

$$B^S(x) = \begin{pmatrix} 1 & 0 & 0 & 0 & 0 & 0 \\ b_{21} & b_{22} & b_{23} & 0 & 0 & 0 \\ 0 & 0 & b_{33} & 0 & 0 & 0 \\ 0 & 0 & 0 & -1 & 0 & 0 \\ 0 & 0 & 0 & b_{54} & b_{55} & b_{56} \\ 0 & 0 & 0 & 0 & 0 & b_{66} \end{pmatrix} \quad C^S(x) = \begin{pmatrix} 0 & 0 & 0 & 0 & 0 & 0 \\ c_{21} & c_{22} & c_{23} & 0 & 0 & 0 \\ c_{31} & c_{32} & c_{33} & 0 & c_{35} & c_{36} \\ 0 & 0 & 0 & 0 & 0 & 0 \\ 0 & 0 & 0 & c_{54} & c_{55} & c_{56} \\ 0 & c_{62} & c_{63} & c_{64} & c_{65} & c_{66} \end{pmatrix}$$

Note that:

- the superscript S is for steady state
- The entries of the matrices $A^S(x), B^S(x), C^S(x)$ are given in section A.2.1 of the appendix.

The linear system with space varying coefficients (3.4), is simplified by averaging over the whole domain the matrices ($A^S(x)$,$B^S(x), C^S(x)$). System (3.4) then becomes:

$$\bar{A^S}\frac{\partial W}{\partial t} + \bar{B^S}\frac{\partial W}{\partial x} + \bar{C^S}W = 0 \tag{3.5}$$

Where $\bar{A^S}, \bar{B^S}, \bar{C^S}$ are the average of $A^S(x), B^S(x), C^S(x)$ over the whole space, respectively.

3.2.1 Linearized model simulation

In simulation, linearization error between the systems (2.1)-(2.6) and (3.5) is addressed. The two systems are simulated starting with the same initial condition. This initial condition is considered far enough from the steady state. The relative errors plotted are of the following form:

$$\varepsilon_X^{H/C}(t) = \frac{\int_0^1 |X_{NL}^{H/C}(x,t) - X_L^{H/C}(x,t)|dx}{\int_0^1 X_S^{H/C}(x)dx}$$

where X is the mass flow rate, pressure or enthalpy.
Note:

- X_{NL}: represents the output of the nonlinear model
- X_L: represents the output of the linearized-averaged model
- The numerical scheme used in the simulation for approximating the first order spatial derivative $\frac{\partial W}{\partial x}$ is the forward and backward finite difference depending on the flow direction.

The results are presented in figure (3.1).

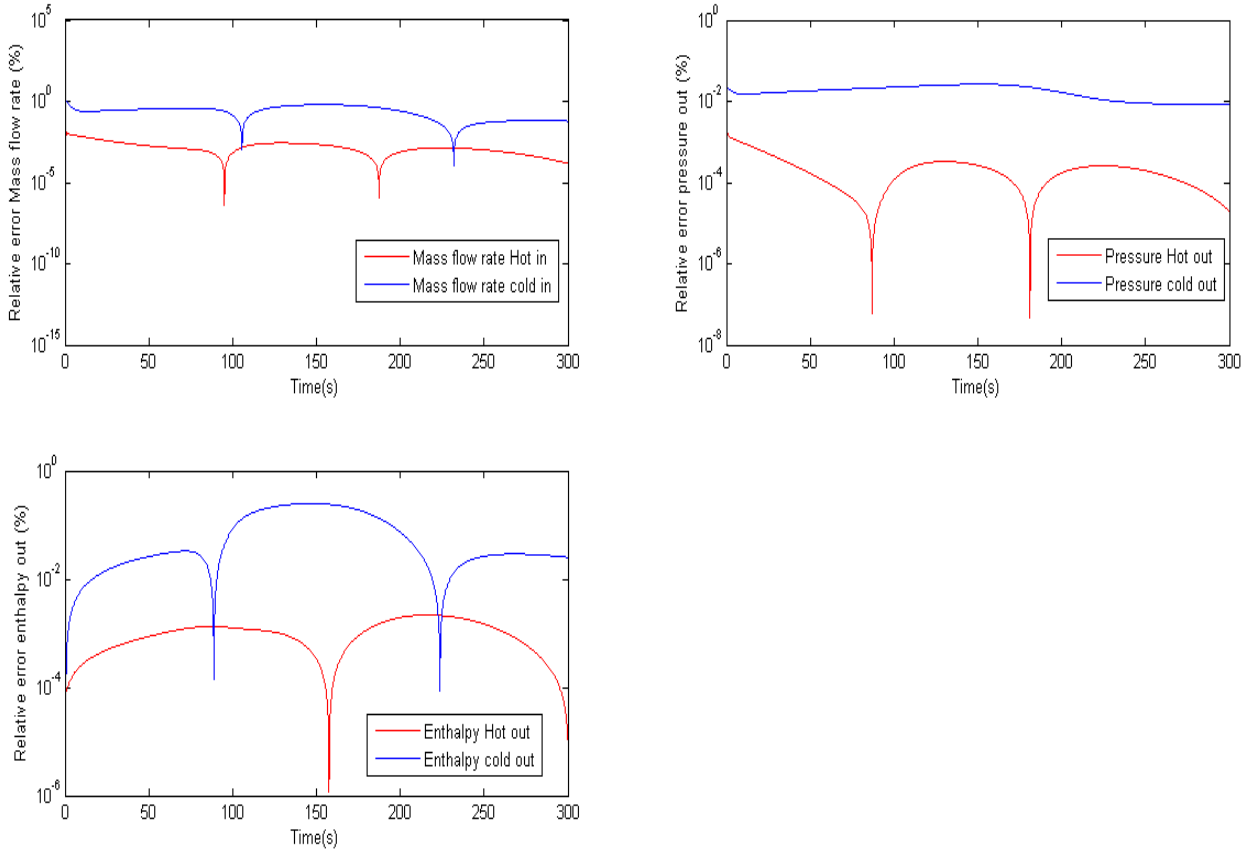

FIGURE 3.1: Output Relative Error

The error plots above, show that the linearization is highly accurate. The error in the different plots is less than 10%. We can conclude that the non linearity didn't play an important role in our working range and the linearized-averaged model (3.5) captures all the necessary dynamics of the system.

3.3 Observer Architecture

The averaged linearized system (3.5), is now manipulated in a control oriented way in preparation for the observer design .The idea here is to diagonalize system (3.5) in order to decouple the space derivative of the states from each other. First system (3.5) is multiplied by $(A^{\bar{S}})^{-1}$ and we have that:

$$\frac{\partial W}{\partial t} + M\frac{\partial W}{\partial x} = NW \tag{3.6}$$

Where $M = (A^{\bar{S}})^{-1}\bar{B^S}$ and $N = -(A^{\bar{S}})^{-1}\bar{C^S}$. $(A^{\bar{S}})^{-1}$ is full rank as long as the density ρ is not constant with respect to time. Then the state W is transformed into the decoupled state U by the transformation T as follows:

$$\begin{aligned} W &= TU \\ \Lambda &= T^{-1}MT \\ F &= T^{-1}NT \end{aligned} \tag{3.7}$$

Such that: $\Lambda = diag\{\lambda_1..\lambda_6\}$ and F is arbitrary, where ($\lambda_1 > 0, \lambda_3 > 0, \lambda_5 > 0$) and ($\lambda_2 < 0, \lambda_4 < 0, \lambda_6 < 0$). For each fluid we have mass and energy flow in one direction and momentum in the reverse direction. As hot and cold go in opposite directions, we have 3 positive and 3 negative Eigenvalues. Then system (3.6) becomes:

$$\frac{\partial U}{\partial t} + \Lambda\frac{\partial U}{\partial x} = FU \tag{3.8}$$

Note: The state U has no physical meaning, so in order to implement the boundary conditions for the transformed system, the sign of the eigen values is used. If the eigen value is positive then there should be a boundary condition implemented at 0 and if it is negative the boundary condition is implemented at 1. Then the boundary conditions of (3.8) are as follows:

$$\begin{aligned} U_1(0,t) &= g_1(t) \qquad U_2(1,t) = g_2(t) \\ U_3(0,t) &= g_3(t) \qquad U_4(1,t) = g_4(t) \\ U_5(0,t) &= g_5(t) \qquad U_6(1,t) = g_6(t) \end{aligned} \tag{3.9}$$

$g_1, g_2, g_3, g_4, g_5, g_6$ are calculated using the transformation T: $U(0,t) = T^{-1}W(0,t)$ and $U(1,t) = T^{-1}W(1,t)$.

System (3.8) with boundary conditions (3.9) is proved observable and controllable by [17] and as our objective is to estimate the state U from boundary measurements, then the only information we have is coming from the boundary. A natural choice for the observer architecture is:

$$\frac{\partial \hat{U}}{\partial t} + \Lambda\frac{\partial \hat{U}}{\partial x} = F\hat{U} \tag{3.10}$$

Let's define the following left and right matrices

$$M_l = \begin{pmatrix} 1 & 0 & 0 & 0 & 0 & 0 \\ 0 & 0 & 1 & 0 & 0 & 0 \\ 0 & 0 & 0 & 0 & 1 & 0 \end{pmatrix} \quad M_r = \begin{pmatrix} 0 & 1 & 0 & 0 & 0 & 0 \\ 0 & 0 & 0 & 1 & 0 & 0 \\ 0 & 0 & 0 & 0 & 0 & 1 \end{pmatrix}$$

with $U_l(0,t) = M_l T^{-1} W(0,t)$, $U_r(1,t) = M_r T^{-1} W(1,t)$. The observer boundary conditions become

$$\begin{aligned} \hat{U}_l(0,t) &= U_l(0,t) + 1_{3\times 3} M_r L(U(0,t) - \hat{U}(0,t)) \\ \hat{U}_r(1,t) &= U_r(1,t) + 1_{3\times 3} M_l L(U(1,t) - \hat{U}(1,t)) \end{aligned} \tag{3.11}$$

where $L = diag\{L_1, .., L_6\}$, $1_{3\times 3}$: ones matrix (3×3) . The inflow boundary conditions are thus corrected by the error of the outflows boundaries, and the same is done for the outflow observer boundaries which are corrected by the errors of the inflow boundaries. All the errors are weighted by the observer gains L_1 to L_6.

3.3.1 Global Exponential Stability (GES)

In this section, we prove the global exponential convergence of the observer (3.10) with boundary conditions (3.11). This is done by proving the exponential convergence of the estimated error $\varepsilon(x,t) = U(x,t) - \hat{U}(x,t)$ towards zero. Let us start by considering the error dynamics:

$$\frac{\partial \varepsilon}{\partial t} + \Lambda \frac{\partial \varepsilon}{\partial x} = F\varepsilon \tag{3.12}$$

with the following boundary conditions:

$$\begin{aligned} \varepsilon_l(0,t) &= -1_{3\times 3} M_r L \varepsilon(0,t) \\ \varepsilon_r(1,t) &= -1_{3\times 3} M_l L \varepsilon(1,t) \end{aligned} \tag{3.13}$$

The authors in [11] consider the problem of stability and control synthesis for first order quasi-linear hyperbolic systems. The exponential stability is proved by a Lyapunov candidate constrained by satisfying certain set of MIs (Matrix inequalities).

Definition 3.1. System (3.12)-(3.13) is said to be *Globally Exponentially Stable* if there exist $\gamma > 0$ and $C > 0$ such that for every initial condition $\varepsilon^0 \in L^2((0,1); R^6)$ the solution of the system (3.12)-(3.13) satisfies:

$$|\varepsilon(t,.)|_{L^2((0,1);R^6)} \leq Ce^{-\gamma t} |\varepsilon^0|_{L^2((0,1);R^6)} \tag{3.14}$$

Consider the following Lyapunov candidate, similar to the one used in [11]:

$$V(\varepsilon) = \int_0^1 \varepsilon^T(x) |\Lambda|^{-1} Q(x) \varepsilon(x) dx \tag{3.15}$$

where $\mu \in R$, $|\Lambda|^{-1} = diag[1/|\Lambda_i|]$ and $Q(x) = diag[q_i e^{-sign(\Lambda_i)2\mu x}]$ for all $i \in \{1, \ldots, 6\}$. The convergence of our observer can be inferred from the following theorem.

Theorem: Consider the system of PDEs (3.12) with boundary conditions (3.13). Suppose that there exist $\gamma > 0$, $\mu \in R$, and a positive definite matrix $Q(x) > 0$ such that for all $x \in [0,1]$ we have:

$$F^T |\Lambda|^{-1} Q(x) + |\Lambda|^{-1} Q(x) F - 2\mu Q(x) \leq -2\gamma |\Lambda|^{-1} Q(x) \tag{3.16}$$

$$\begin{pmatrix} -q_2^0+\alpha L_2^2 & \alpha L_2 L_4 & \alpha L_2 L_6 & 0 & 0 & 0 \\ * & -q_4^0+\alpha L_4^2 & \alpha L_4 L_6 & 0 & 0 & 0 \\ * & * & -q_6^0+\alpha L_6^2 & 0 & 0 & 0 \\ 0 & 0 & 0 & -q_1^1+\beta L_1^2 & \beta L_1 L_3 & \beta L_1 L_5 \\ 0 & 0 & 0 & * & -q_3^1+\beta L_3^2 & \beta L_3 L_5 \\ 0 & 0 & 0 & * & * & -q_5^1+\beta L_5^2 \end{pmatrix} \leq 0 \qquad (3.17)$$

where q_i^0 and q_i^1 for $i \in \{1,\ldots,6\}$ are the diagonal entries of $Q(0)$ and $Q(1)$ respectively, $\alpha = q_1^0+q_3^0+q_5^0$ and $\beta = q_2^1+q_4^1+q_6^1$.

Then (3.12) with (3.13) is (GES). The proof is done in section (A.2.2) of the appendix.

3.4 Simulation Results

The performance of the proposed observer architecture is evaluated with simulations by comparing against the output of the nonlinear model. The model starts at steady state and is excited by step variations in the inlet hot temperature (this kind of boundary change is realistic when dealing with the real system as discussed in Chapter 4).

The observer gains are calculated as follows:

- Equation (3.16) is an infinite LMI. To calculate the matrix $Q(x)$, the polytopic approach proposed by [11] is used.
- In the polytopic approach, first $\mu > 0$ and $\gamma > 0$ are chosen, then equation (3.16) is solved using the *Yalmip toolbox (Matlab)* to calculate $Q(0)$.
- LMI (3.16) is rechecked for $Q(1)$ and Q_{01} to satisfy negative definiteness. Where, Q_{01} is obtained from $Q(x)$ by substituting $x = 0$ in the i^{th} entry if $(sign(\Lambda_i) < 0)$, and $x = 1$ otherwise.
- In (3.17), we proceed by trial and error. We first ensure that the diagonal elements are negative and then adjust the gains to satisfy the MI.

Equation (3.16) is solved for $\mu = 1.5$ and $\gamma = 0.01s^{-1}$, and the values of the observer gains obtained are :

$$\begin{array}{ll} L_1 = 0.0092 & L_2 = 0.3276 \\ L_3 = 0.0104 & L_4 = 0.2141 \\ L_5 = 0.0058 & L_6 = 0.3943 \end{array}$$

The simulation is done in 3 scenarios: First starting close to steady-state by a near estimated initial condition, second starting with far estimated initial condition and the last one checking the robustness of the observer by adding noise to the measurements. In all 3 scenarios, a step decrease (1.7 °C) in the hot inlet temperature is applied at T = 1500s.

- First Scenario: Initial Condition Close to Steady State

  The set of initial conditions used is:

$$\begin{array}{ll} T^H(0,x) = T_H^S(x) & \hat{T}^H(0,x) = T_H^S(x) + 0.23\ °\mathrm{C} \\ T^C(0,x) = T_C^S(x) & \hat{T}^C(0,x) = T_C^S(x) + 0.12\ °\mathrm{C} \\ P^H(0,x) = P_H^S(x) & \hat{P}^H(0,x) = T_H^S(x) + 0.15MPa \\ P^C(0,x) = P_C^S(x) & \hat{P}^C(0,x) = P_C^S(x) + 6000(Pa) \\ \dot{m}^H(0,x) = 0.02Kg/s & \hat{\dot{m}}^H(0,x) = 0.02Kg/s \\ \dot{m}^C(0,x) = 0.02Kg/s & \hat{\dot{m}}^C(0,x) = 0.0194Kg/s \end{array}$$

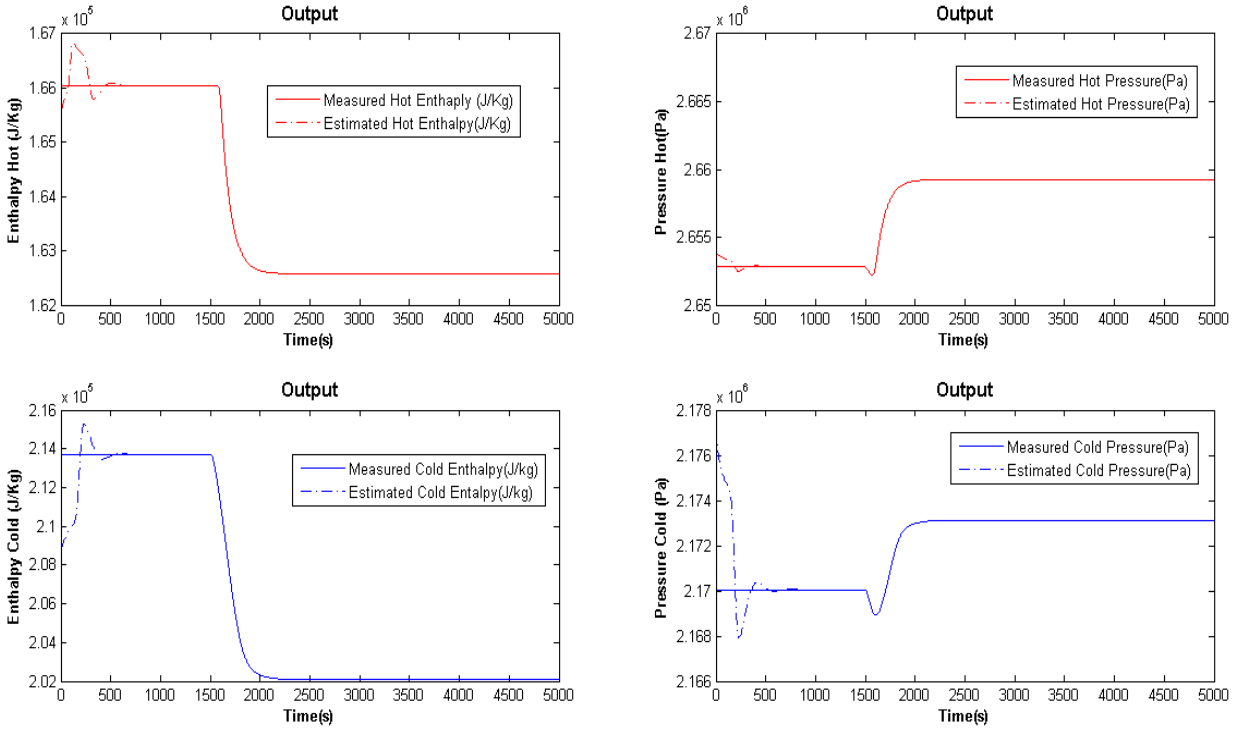

FIGURE 3.2: Enthalpy-Pressure Estimation

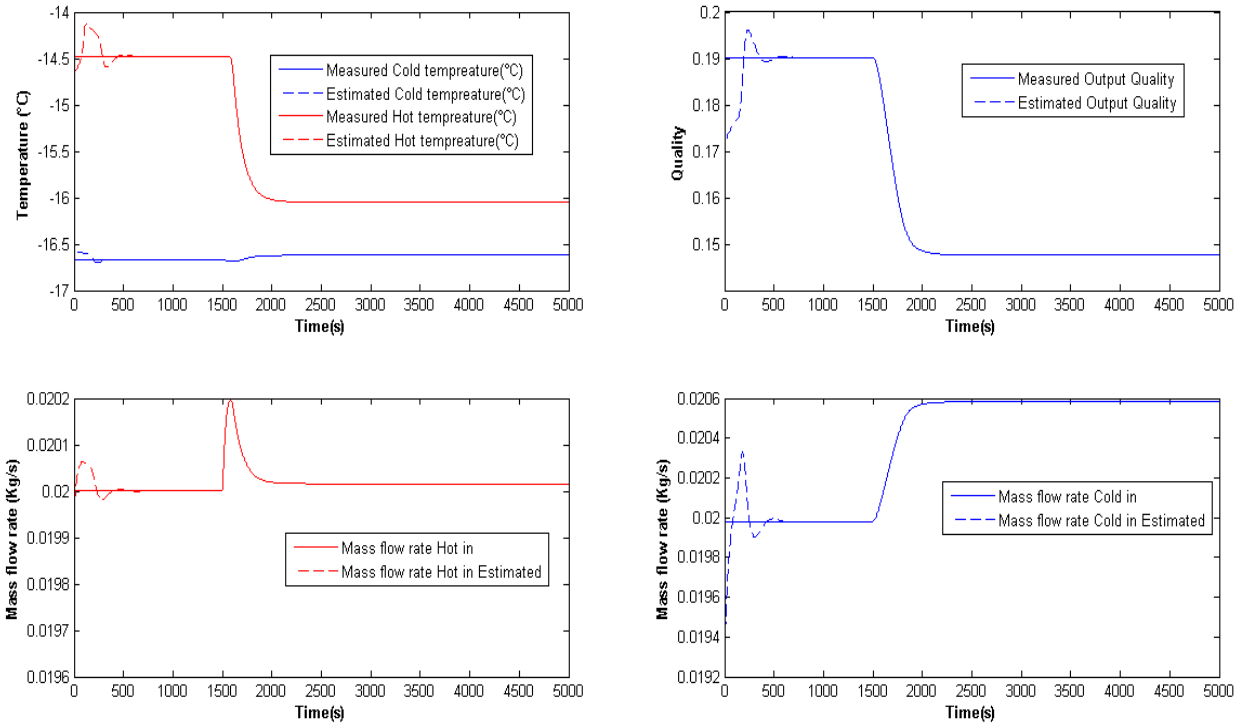

FIGURE 3.3: Mass Flow Rate, Temperature and Quality Estimation

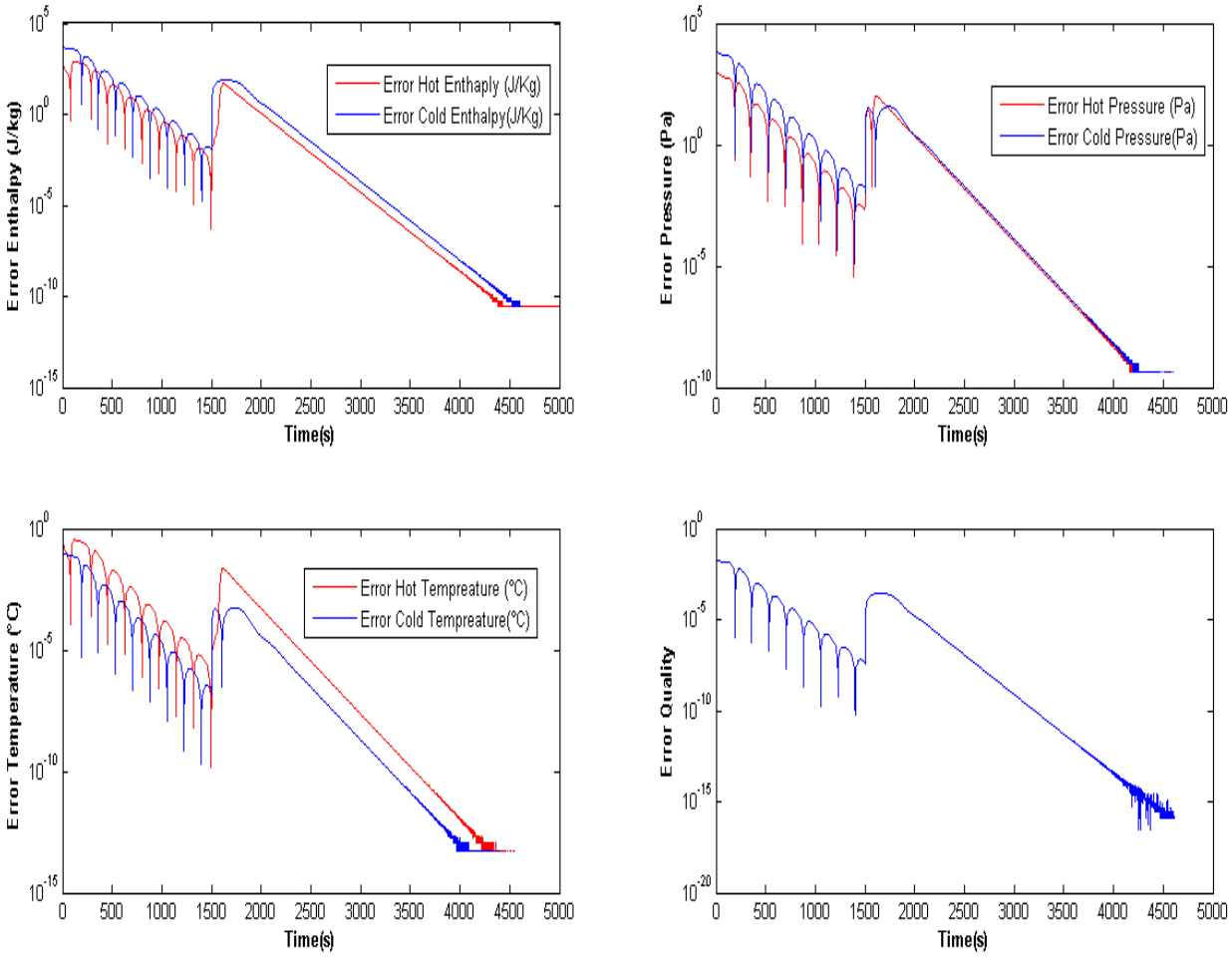

FIGURE 3.4: Estimation Error (Near Initial Condition)

The boundary conditions are the same as used in (2.7), but at T=1500s a filtered step decrease of (1.7 °C) in the input hot temperature is done. As shown in Fig (3.2) and (3.3), the observer converges with slight overshoot. Regarding the estimation errors in Fig (3.4), we have an exponential decay towards zero, but with small amplitude oscillations at the start. The spikes are due to the intersection of the model with the estimated values. When the step is triggered, an increase in the error happened since the step is very fast so the observer takes time to react and then the error starts again to decay. The decay rate predicted is γ= 0.01 s^{-1} while we get 0.0033 s^{-1} (from the simulation), this issue should be addressed in future works.

- Second Scenario: Far Estimated initial Condition
  The set of initial conditions used is:

$$
\begin{array}{ll}
T^H(0,x) = T^S_H(x) & \hat{T}^H(0,x) = T^S_H(x) - 2.23\ ^\circ\mathrm{C} \\
H^C(0,x) = H^S_C(x) & \hat{H}^C(0,x) = H^S_C(x) - 30(KJ/Kg) \\
P^H(0,x) = P^S_H(x) & \hat{P}^H(0,x) = T^S_H(x) + 0.05MPa \\
P^C(0,x) = P^S_C(x) & \hat{P}^C(0,x) = P^S_C(x) + 6000(Pa) \\
\dot{m}^H(0,x) = 0.02Kg/s & \hat{\dot{m}}^H(0,x) = 0.021Kg/s \\
\dot{m}^C(0,x) = 0.02Kg/s & \hat{\dot{m}}^C(0,x) = 0.0196Kg/s
\end{array}
$$

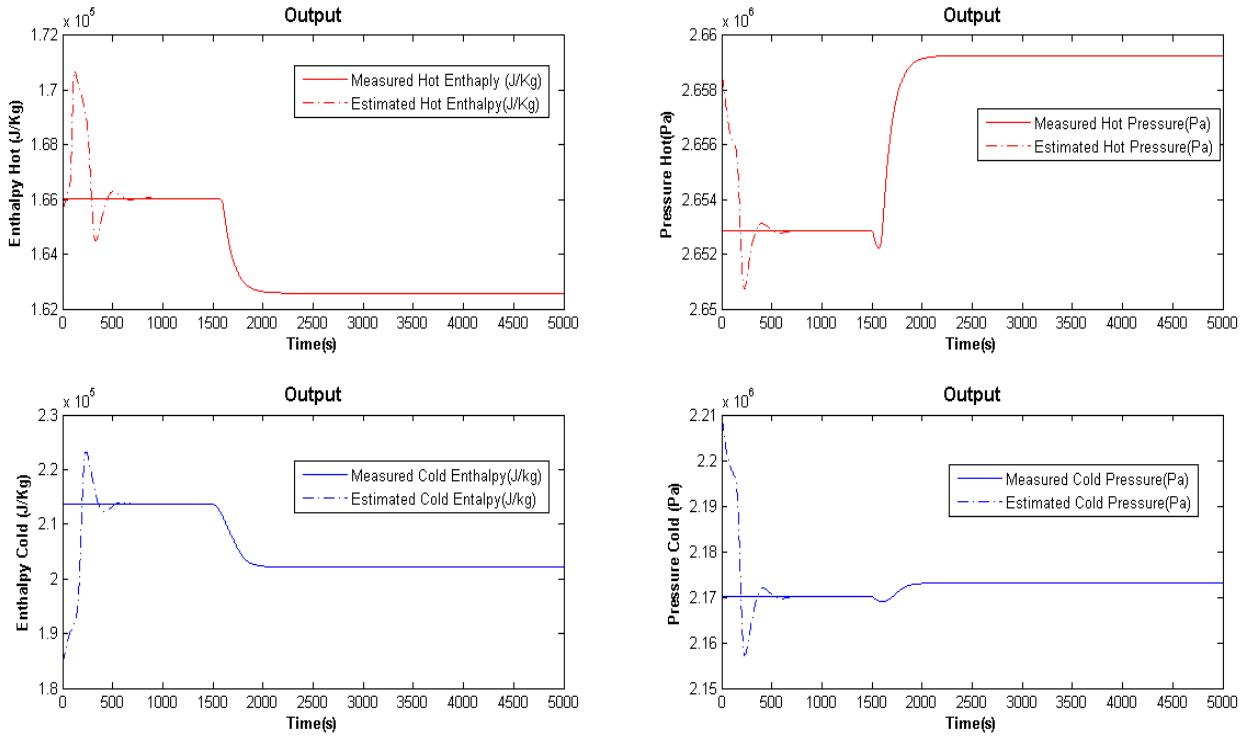

FIGURE 3.5: Enthalpy-Pressure Estimation

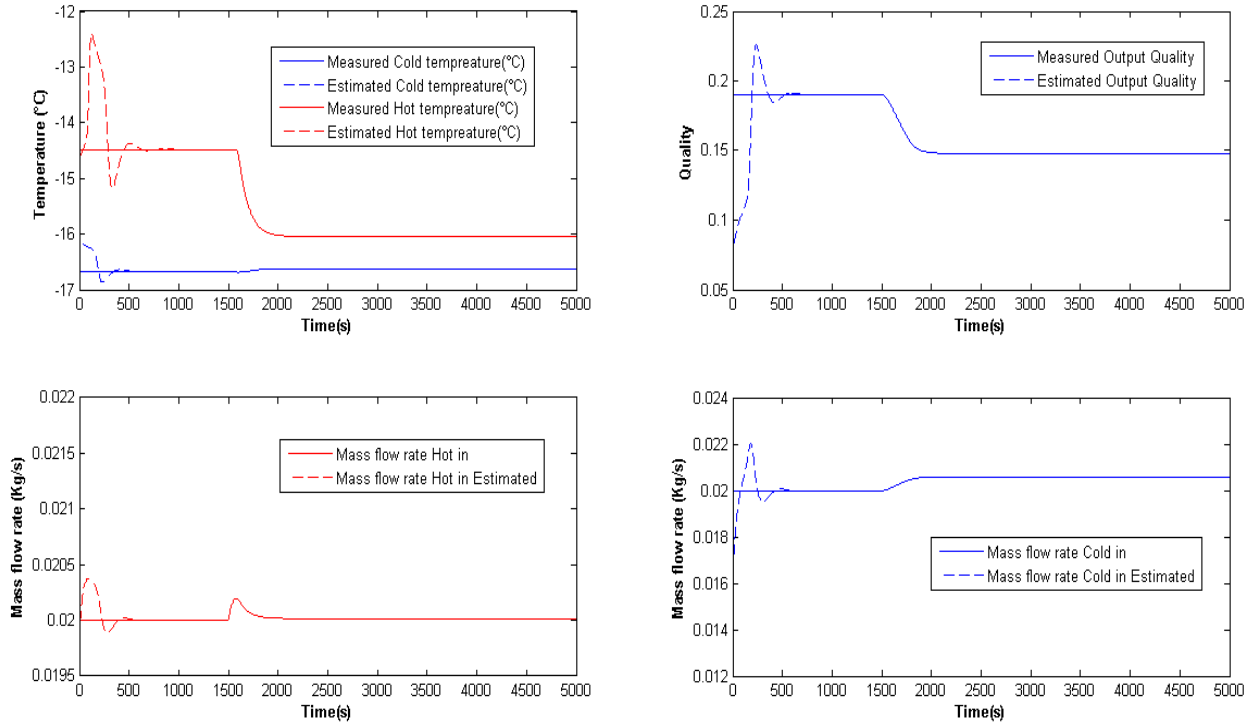

FIGURE 3.6: Mass Flow Rate, Temperature and Quality Estimation

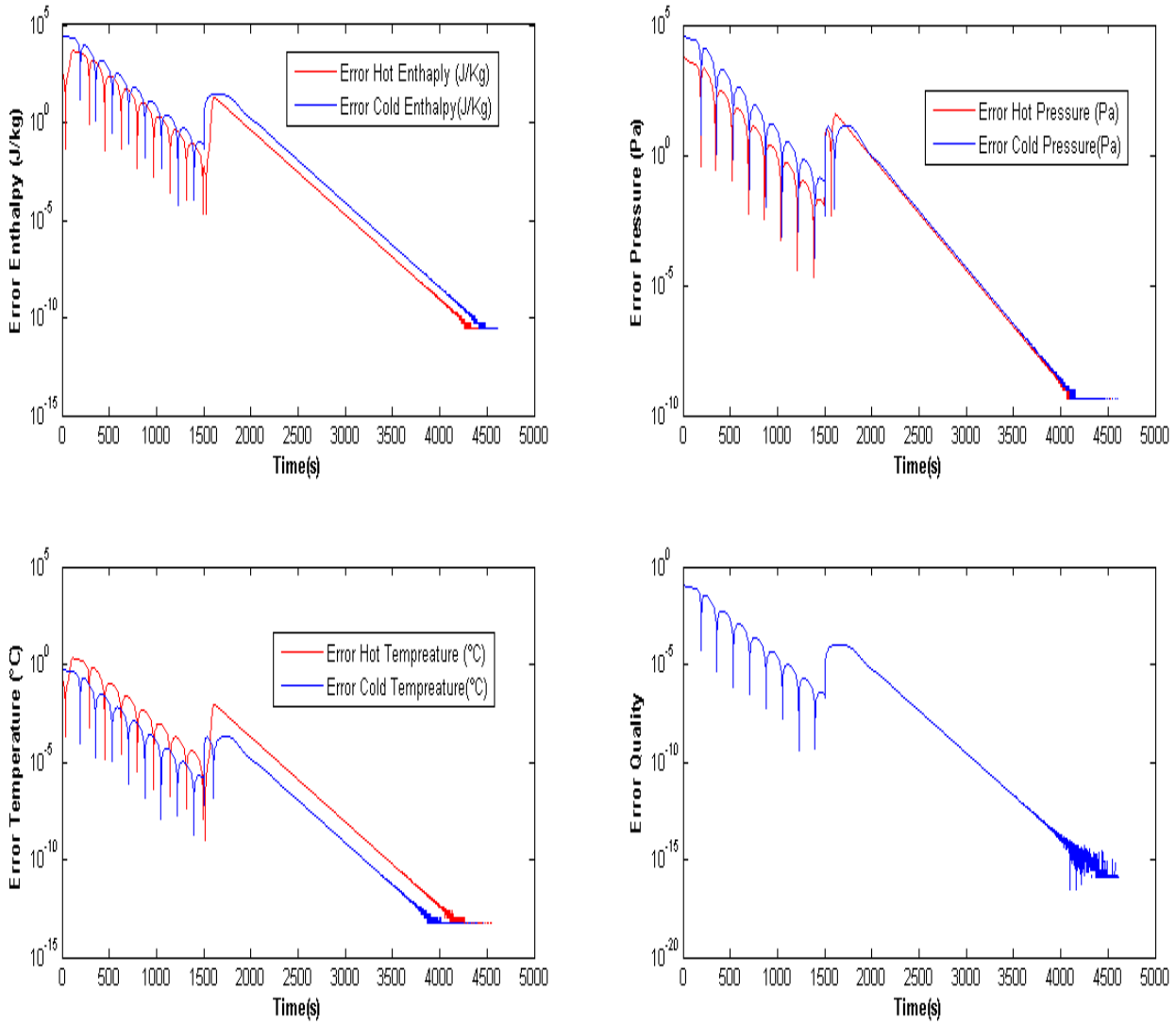

FIGURE 3.7: Estimation Error (Far Initial Condition)

Since the pressure interval is constrained between [2MPa,3MPa], then the range of temperatures will be also constrained and as the mass flow rate is constant along the tubes at steady state, it remain to change the estimated quality by modifying the cold enthalpy. The cold enthalpy is decreased by (30KJ/kg). As shown in Fig (3.5)-(3.6), the observer still converges toward the model, starting with high amplitude oscillations. Error convergence is also exponential in Fig (3.7), but since the convergence rate is constant, the observer take longer time to converge because of the high estimation error at the beginning , this appears clearly in the temperature plots (3.6).

- Third Scenario: Addition of Noise Measurements

  The set of initial conditions used are the same as the second scenario.

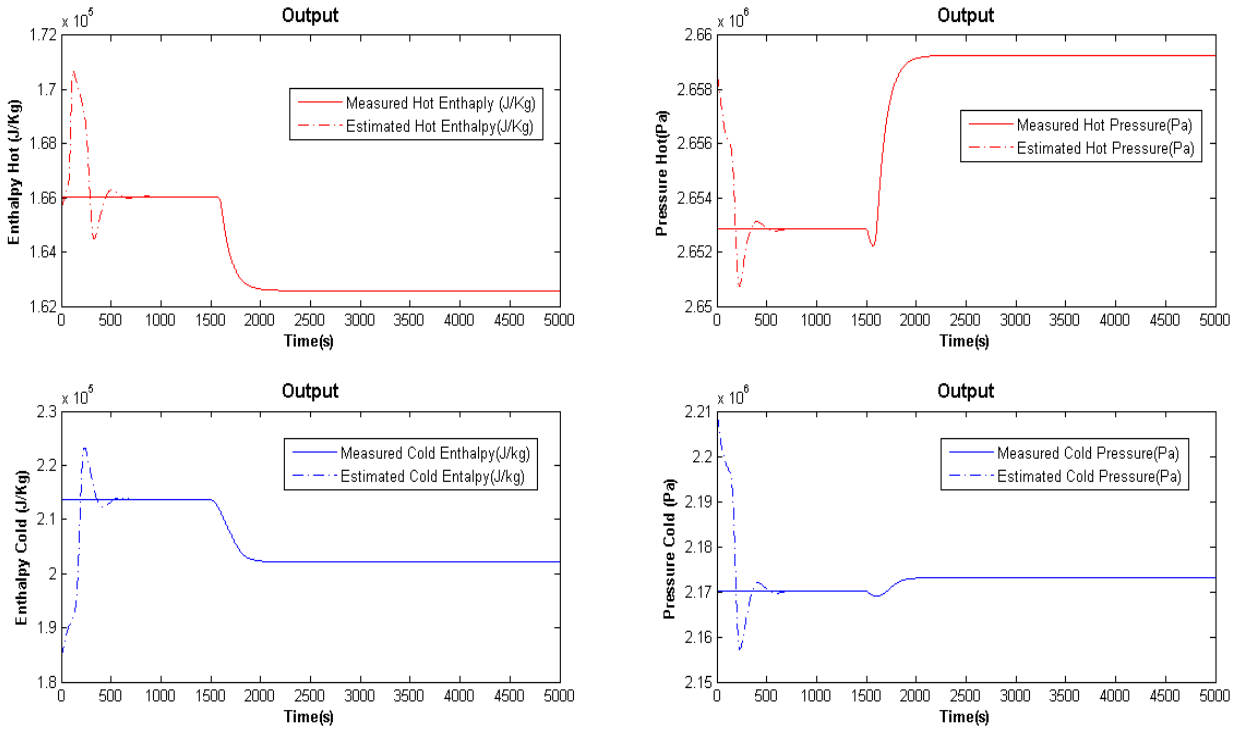

FIGURE 3.8: Enthalpy-Pressure Estimation

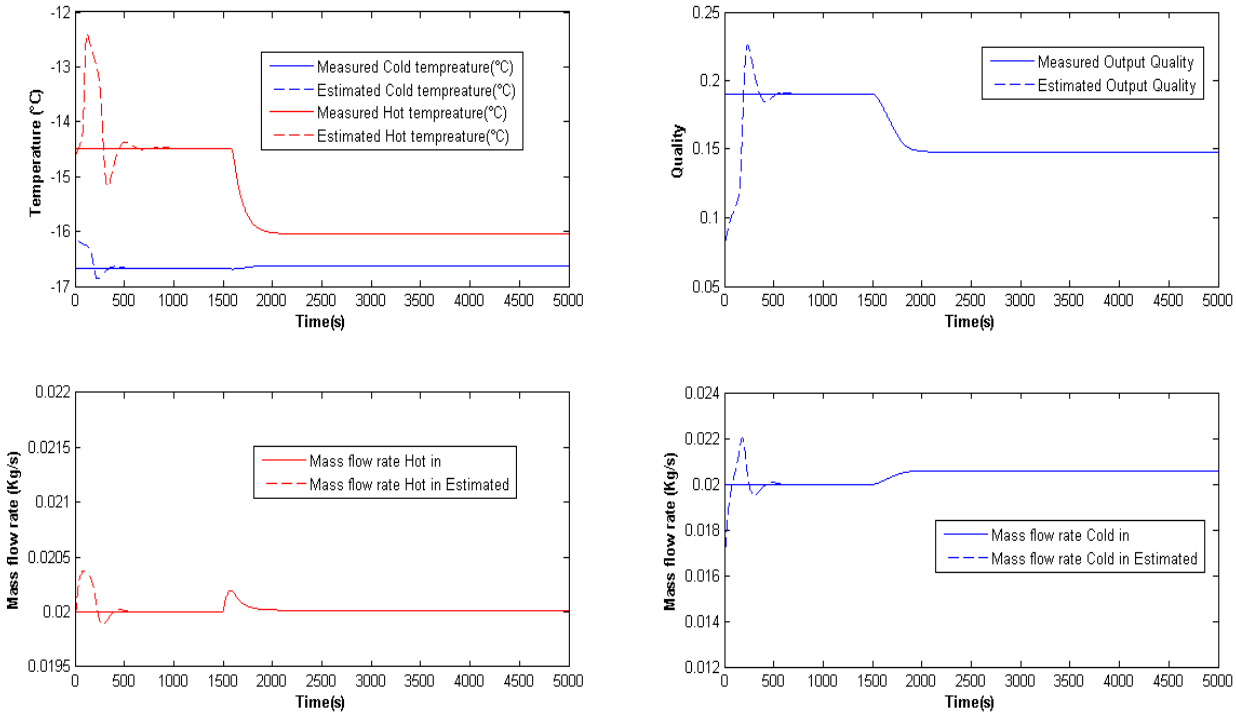

FIGURE 3.9: Mass Flow Rate, Temperature and Quality Estimation

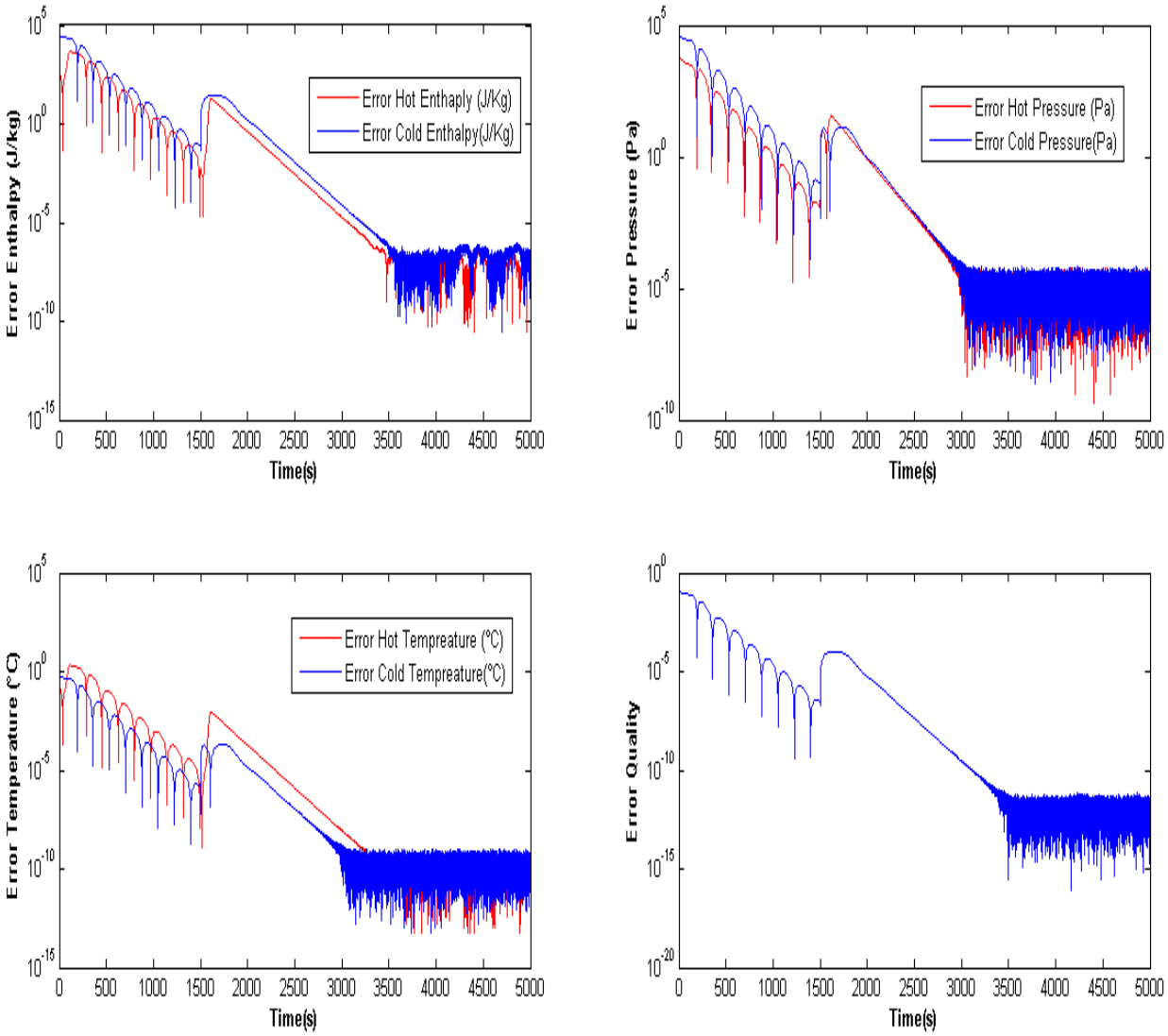

FIGURE 3.10: Estimation Error (Addition of Noise Measurements)

An additive white Gaussian noise is added to the measurements used by the observer such that the signal to noise ratio $(SNR = 100)$, the simulated results are plotted in Fig (3.8)-(3.9)-(3.10). The error plots show that the observer converges exponentially to a minimum value determined by the noise amplitude (steady state error). The noises are attenuated and we can deduce that our observer is reasonably robust against measurement noises.

3.5 Conclusion

The simulation results clearly agrees with the theory made on the observer exponential convergence. The next step is to validate our observer experimentally on the actual system found at *CERN, Switzerland*. This is extensively explained in the next chapter.

Chapter 4

Experimental Validation

4.1 Introduction

The previous chapters have shown the extensive theory of the observer design. As the simulation results were reasonably logical, a mission to *CERN, Geneve* was ordered to validate experimentally our work. The aim of this chapter is to show the overall experimental setup of the system with the experiments done on it. As a result, our model is adapted to this setup and the results are compared against the experimental values.

4.2 Experimental Setup

First the real simulator that uses PLC to control the plant is presented in Fig (4.1).The cold fluid is pumped by the pump (LP3004) to the transfer lines and then heated by means of two heaters (EH7027) and (EH7028) to have the hot fluid. Both hot and cold fluid exchange heat through these lines and finally the hot fluid is cooled down by the chiller (HX3082) to be pumped again by the pump. The point of interest for us in this system is the transfer line, this line is the concentric tube exchanger and sensors located at the boundaries are our measurement sensors.The real plant setup is presented in Fig (4.2), Fig (4.3) and Fig (4.4) . This system was build to run educative experiments for developing and improving CO_2 cooling technology. It's seen that the transfer line in Fig (4.2) is long enough for the heat exchange, not straight but can be assumed straight due to the very low pressure drop as we will see in the next sections.

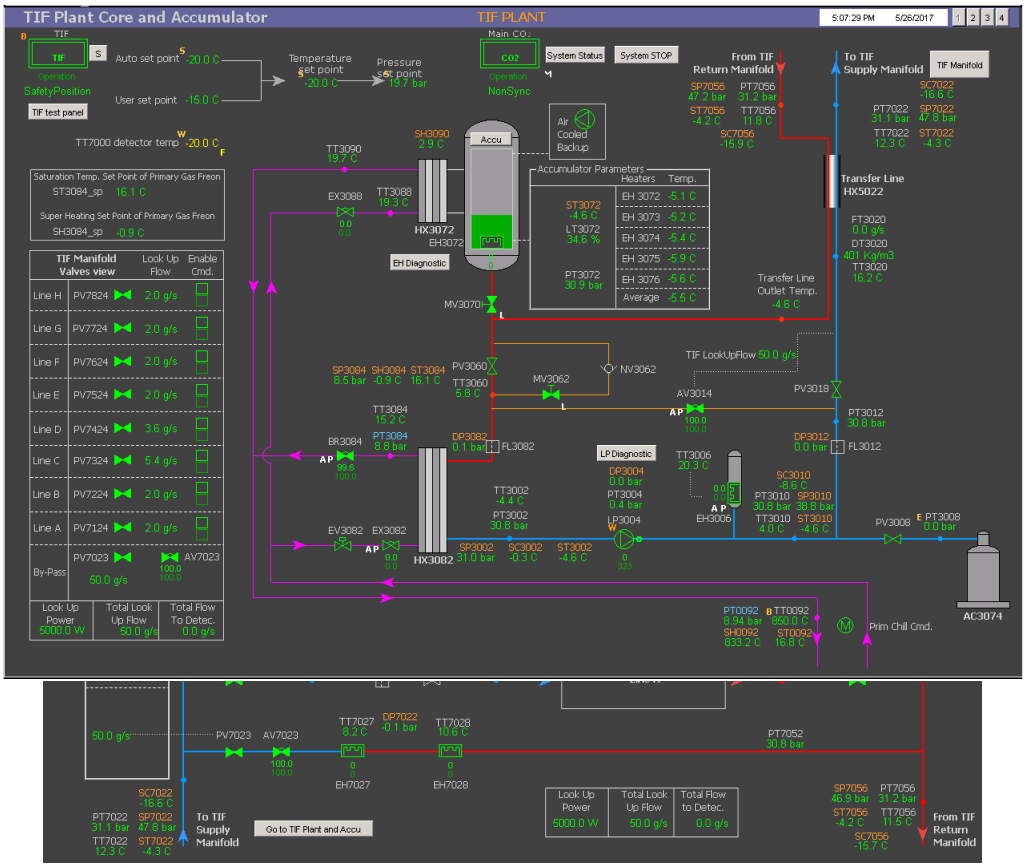

FIGURE 4.1: PLC Control Program

FIGURE 4.2: 15KW CO_2 Cooling System

FIGURE 4.3: Sensors

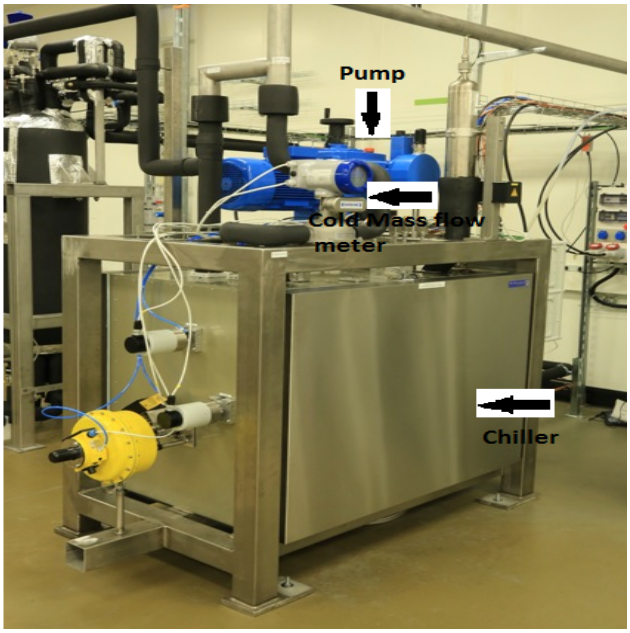

FIGURE 4.4: Pump- Mass flow meter- Chiller

4.2.1 Experiment and Collected Measurements

The above system is designed to work with two phase, but for technical reasons we were allowed to make the experiments in single phase only. As a result liquid is circulated everywhere in the system: both the cold and hot fluids enter at liquid phase and remain so.

As the considered system is the transfer line that carry the hot and cold fluids, the sensors that are located at the boundaries of the tube are:

- FT3020: Measure the inlet cold mass flow rate

- PT3012: Measure the inlet cold pressure
- TT3020: Measure the inlet cold temperature
- PT7022: Measure the outlet cold pressure
- TT7022: Measure the outlet cold temperature
- PT7056: Measure the inlet hot pressure
- TT7056: Measure the inlet hot temperature
- PT3072: Measure the outlet hot pressure
- TT3060: Measure the outlet hot temperature

All the sensors are shown on the figure (4.1). In addition, the 3 variables that can be controlled are:

- **Hot inlet temperature** (Controlled by the amount of heat added by the heaters to the cold fluid)
- **Outlet hot pressure** (Set by the accumulator level)
- **Inlet Cold mass flow rate** (Controlled by the pump speed)

Once the system has reached a steady state, the chosen control parameter is the hot inlet temperature. We vary manually the heating power by several increase and decrease steps trying to have some rich input that can excite all frequencies, the experimental results measured by the sensors are presented in Fig (4.5) and Fig (4.6).

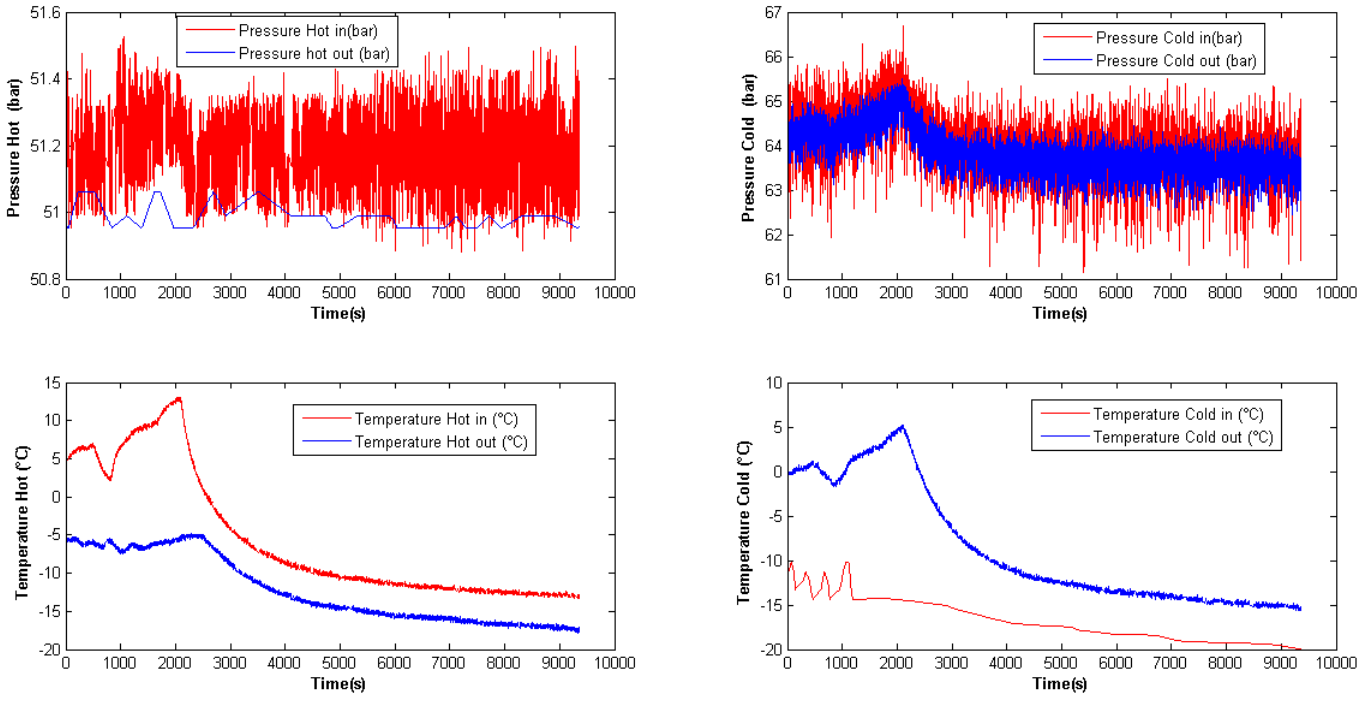

FIGURE 4.5: Temperature-Pressure measurments

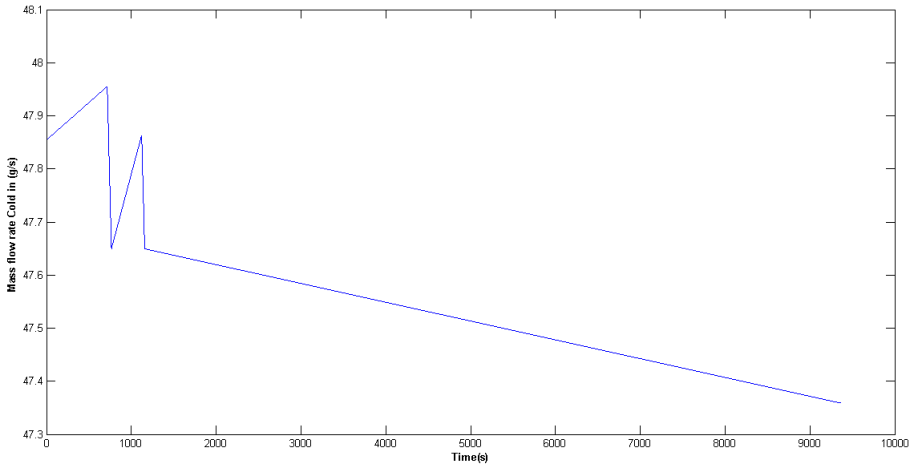

FIGURE 4.6: Mass flow rate Cold in

The experiment is done by modulating the heating power as follows: increase, decrease, increase, increase, decrease as observed in the hot temperature plot Fig (4.5). The severe oscillations in the pressure measurements are due to problems in the pump damper, these oscillations amplitude are greater than the pressure drop along the tube, which makes taking pressures at both boundaries as boundary condition almost impossible.

The proposed solution was: first to smooth the data and then use the valve (AV7023) to calculate the inlet mass flow rate on the hot side by using the equation of the valve . This calculated inlet hot mass flow rate is used as a boundary condition.

- Data Smoothing

  The data is smoothed by the function *movmean* in Matlab that takes the average value on a user defined window. The window used for pressures is 500 (due to the oscillations) and for the temperatures is 50. The sampling time is taken the same as the measurements 1(s). The results are presented in Fig (4.7) and Fig(4.8):

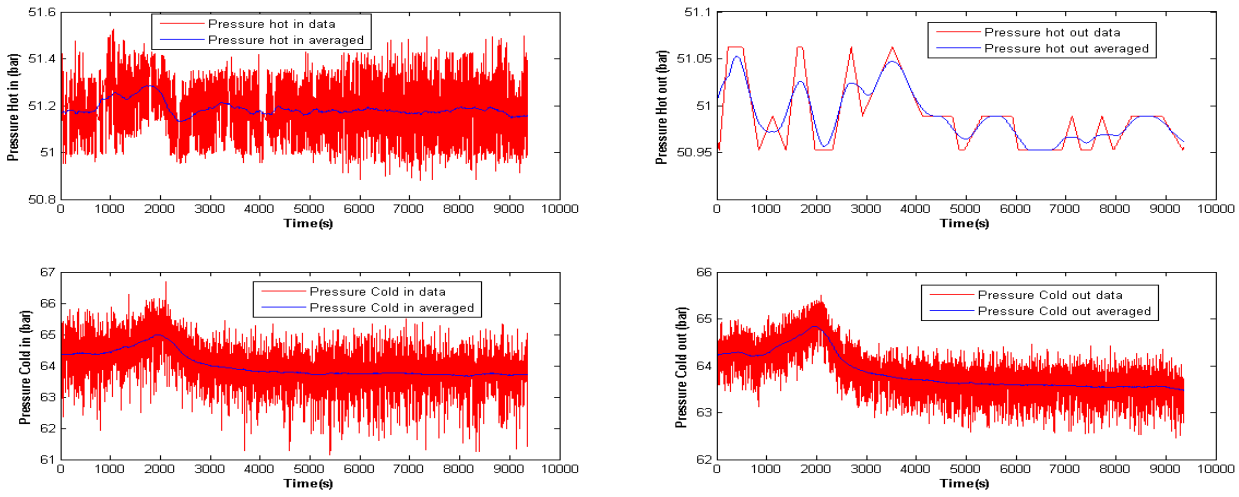

FIGURE 4.7: Smoothed Data- Temperatures

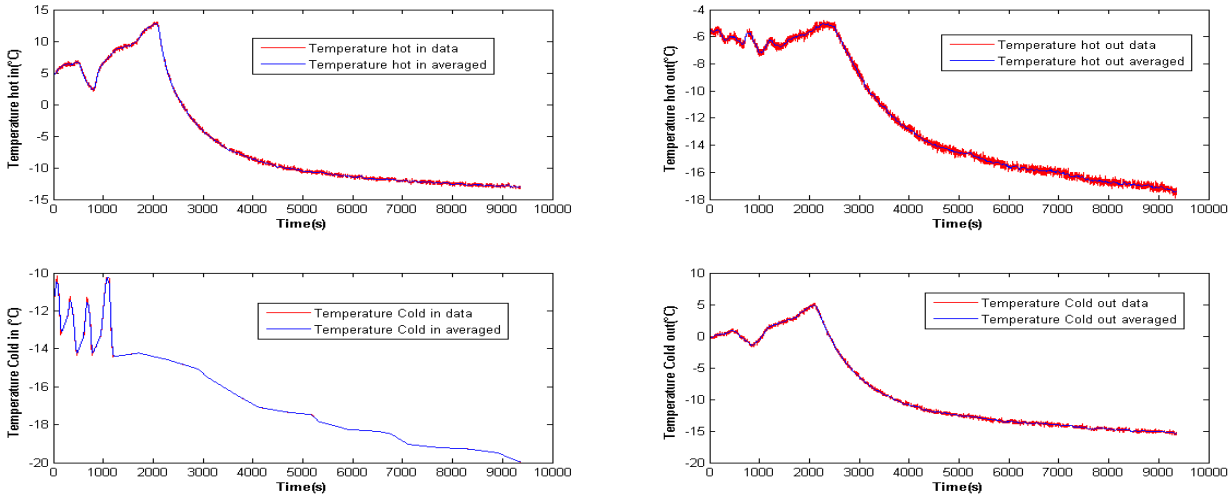

FIGURE 4.8: Smoothed Data- Pressures

- Hot inlet Mass flow rate

  The inlet hot mass flow rate is approximated by a simple equation using the pressure drop across the valve (AV7023) as:

$$\dot{m}_{in}^{H} = 14.5 * \sqrt{P_{out}^{C} - P_{in}^{H}} \tag{4.1}$$

  where 14.5 (g/s) is the nominal mass flow rate across the valve at a pressure difference of 1 bar (given from the data sheet of the valve). Then $\dot{m}_{in}^{H}$ is calculated and smoothed see Fig (4.9).

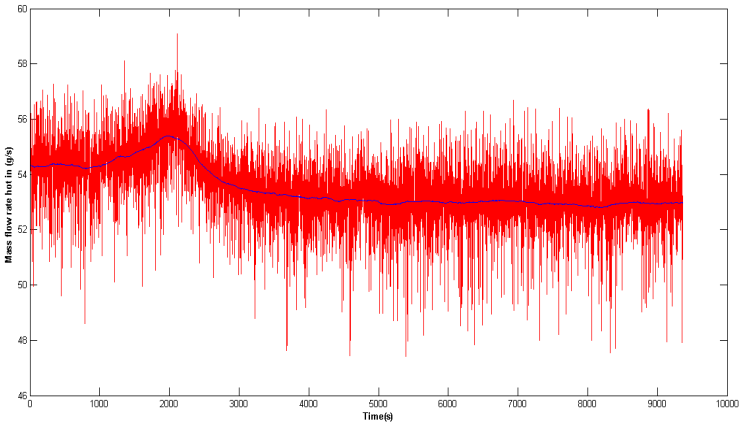

FIGURE 4.9: Inlet Hot Mass Flow Rate

4.3 Model Adaptation

To adapt with the experimental setup discussed above, the model presented in chapters 2 and 3 is changed as follows:

- The two flows are liquid at pressures between (5Mpa-7Mpa), thus only liquid calls are used to calculate the thermodynamic properties

- hot fluid propagates in the outer tube and the cold fluid is in the inside tube
- the boundary conditions are changed from (inlet enthalpy-inlet pressure-outlet mass flow) to (inlet enthalpy-inlet mass flow-outlet pressure)

$$\begin{aligned} H_H(0,t) &= Hin_H & H_c(L,t) &= Hin_C \\ \dot{m}_H(0,t) &= \dot{m}_{in}^H & \dot{m}_C(L,t) &= \dot{m}_{in}^C \\ P_H(L,t) &= P_{out}^H & P_C(0,t) &= P_{out}^C \end{aligned} \tag{4.2}$$

- the model equations (2.1)-(2.6) are slightly modified on the friction pressure drop $\frac{f\dot{m}|\dot{m}|}{2D\rho A}$ which becomes $Af\dot{m}|\dot{m}|$

4.3.1 Heat Transfer and Friction Coefficient Calculations

It's realized during experiments, that the pressure drop on both hot and cold tubes is almost $\Delta P_{nom} = 0.05$ bars at mass flow rates (52 g/s) and (47 g/s) respectively. Using this fact the friction coefficient can be obtained at nominal conditions as:

$$f_{nom} = \frac{\Delta P_{nom}}{\dot{m}_{nom}|\dot{m}_{nom}|} \tag{4.3}$$

For the overall heat transfer coefficient, since the flows are completely liquid, the heat transfer calculation is much simpler than that of the two phase. The idea is to calculate the heat transfer coefficient for both fluids at steady state by Gnielinski correlation [10] and then use a mass flow rate correction to calculate it dynamically. This results in the following equation:

$$\alpha = \frac{1}{\frac{1}{\alpha_H^S(\frac{\dot{m}_H}{\dot{m}_H^S})^{0.8}} + \frac{1}{\alpha_C^S(\frac{\dot{m}_C}{\dot{m}_C^S})^{0.8}}} \tag{4.4}$$

where α_H^S and α_C^S are the hot and cold steady state heat transfer coefficients respectively.

4.3.2 Model Validation

Since the impact of linearization is evaluated previously (Chapter 3), and as our objective is to validate the observer, the model is linearized directly and simulated. By this method, we can infer the accuracy of the linearization when compared to real data. Furthermore, linear steady state distribution is assumed with:

$$\begin{aligned} H_H^S(x) &= \frac{(H_{out}^H - H_{in}^H)}{L}x + H_{in}^H \\ P_H^S(x) &= \frac{(P_{out}^H - P_{in}^H)}{L}x + P_{in}^H \\ H_C^S(x) &= \frac{(H_{in}^C - H_{out}^C)}{L}x + H_{out}^C \\ P_C^S(x) &= \frac{(P_{in}^C - P_{out}^C)}{L}x + P_{out}^C \end{aligned} \tag{4.5}$$

We use inlet temperatures, mass flow rates and outlet pressures as boundary conditions (discussed above). The model evaluation is thus only on the outlet temperatures.

Table 4.1: Numerical values and heat exchanger dimensions

$L = 17.665(m)$	$D_1 = 12(mm)$	$D_2 = 33.4(mm)$
$H_{in}^{H} = 210(KJ/Kg)$	$H_{out}^{H} = 185(KJ/Kg)$	$H_{in}^{C} = 171(KJ/Kg)$
$H_{out}^{C} = 197(KJ/Kg)$	$P_{in}^{H} = 51.17(bar)$	$P_{out}^{H} = 51(bar)$
$P_{in}^{C} = 64.2(bar)$	$P_{out}^{C} = 64.1(bar)$	$\dot{m}_{C}^{S} = 0.047(Kg/s)$
$\dot{m}_{H}^{S} = 0.052(Kg/s)$	$\alpha_{H}^{S} = 370(W/(m^2.K)$	$\alpha_{C}^{S} = 1738(W/(m^2.K)$
$f_1 = 9706(m^{-2}.Kg^{-1})$	$f_2 = 12813(m^{-2}.Kg^{-1})$	$nx = 80(Space - discritization)$

Linearization and averaging are discussed in Chapter 3, we use the same equations (3.3)-(3.5). The initial condition is the same as the steady state distribution (4.5) and the results are presented in Fig (4.10).

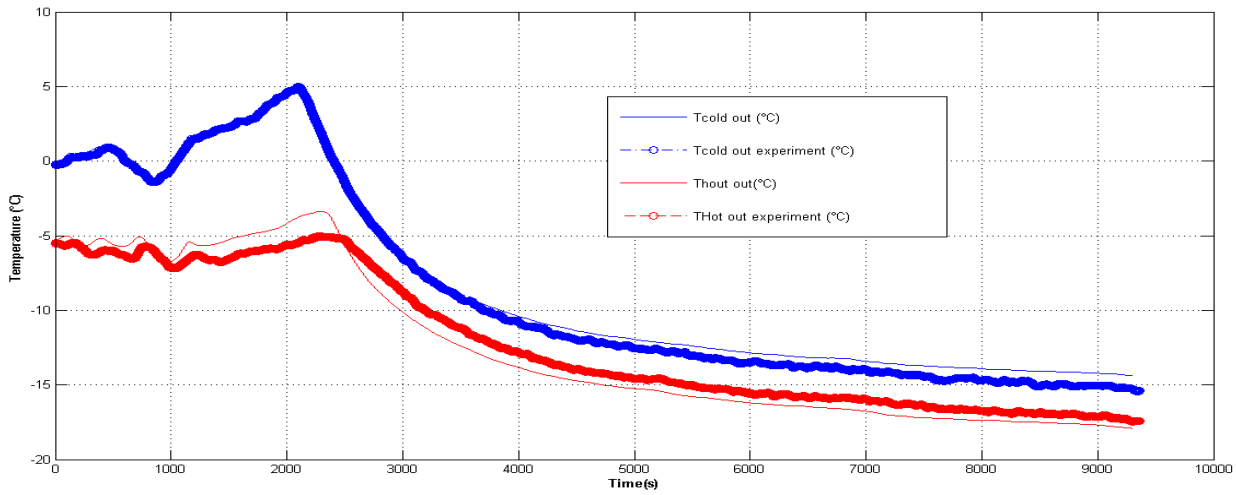

FIGURE 4.10: Outlet Temperatures

Fig (4.10) shows that despite our assumptions, the linearized model outputs are very close to the measured data. The simulation and the measured outputs have the same behavior but the accuracy is better for the cold fluid since we have a measurement from the inlet cold flow meter (FT3020). In contrast, we don't have inlet hot mass flow but we do approximate it using the valve equation (4.1). This appears to be the cause of the slight difference between the measured and simulated outlet hot temperatures.

4.4 Observer Validation

The theory of the observer architecture is all discussed in Chapter 3. It appears that some measurements are not available in the experimental setup. As our model is very close to the experiments, the missing measurements i.e output mass flow rates, inlet pressures (we can't rely on these measurements above due to oscillations) are taken from the model to serve in the calculation of the boundary conditions for the observer. As in Chapter 3, the observer gains are calculated from (3.16) and (3.17) with the parameters from Table (4.1), and the boundary conditions are calculated using the transformation T. The results are presented in Fig (4.11).

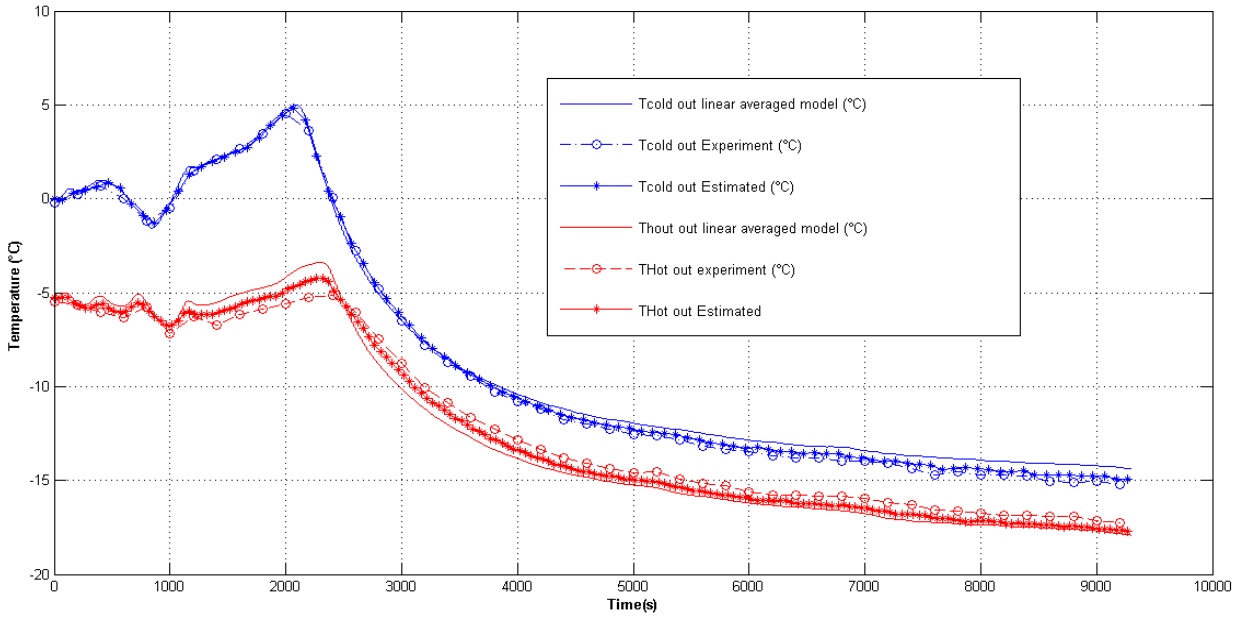

FIGURE 4.11: Estimated Outlet Temperatures

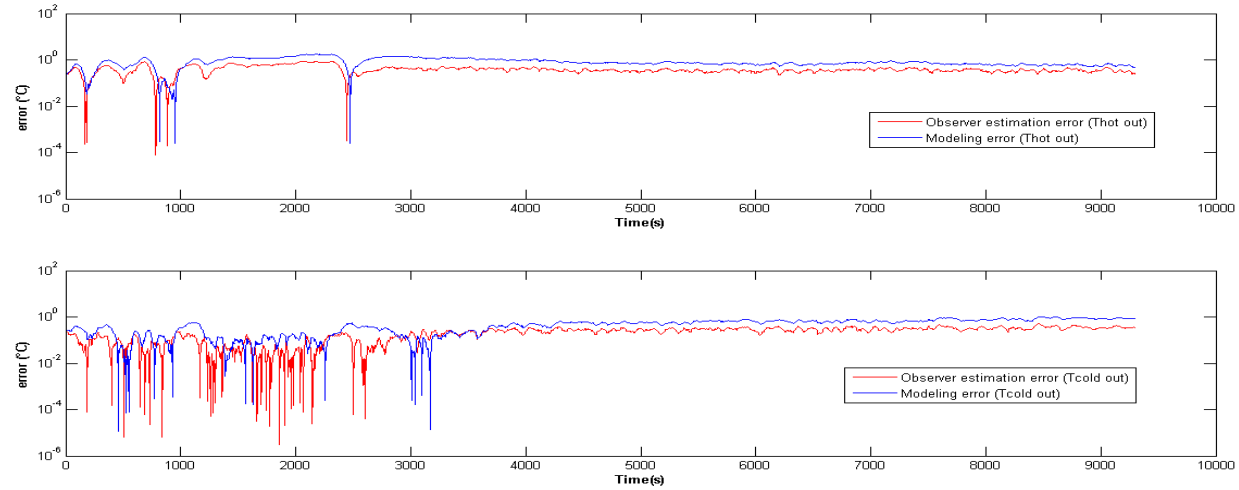

FIGURE 4.12: Estimation Errors

Fig (4.11) shows that the observer corrects the modeling errors and converges more accurately to the experimental data than the linearized-averaged model. In contrast, the estimation error in Fig (4.12) didn't show the requested exponential decay.

4.5 Conclusion

The linearized-averaged model is validated by experiments, this shows that the nonlinearity didn't play an important role. In addition, the observer corrects the modeling errors using measurements taken at the boundaries.

Chapter 5

Conclusion

In this work, the overall objective was to build a boundary observer for two phase CO_2 heat exchanger found at *CERN, Switzerland*. The task of this observer is to estimate the thermodynamic profiles along the tubes of the heat exchanger using measurements taken from the sensors located at the boundaries.

We model the system by using 1D Navier Stokes equations instead of the complex models found in the fluid dynamics literature (3D models, two fluid models..), then the system is linearized around a chosen steady state. The observer is built on these linearized dynamics.

Using a Lyapunov candidate, the estimation error is proved to converge exponentially to zero. This result was assessed by Matlab simulations.

To confirm our results experimentally, test experiments were held at the long CO_2 heat exchanger found at *CERN* but only for single phase flows. Comparison between the real data and simulations shows that the model is significant to predict the dynamical behavior of the flow, then by implementing our observer using the real measurements from the sensors, the observer corrects the modeling errors and converge more accurately to the real data. However, the estimation error didn't converge exponentially to steady state, this needs further investigation.

To conclude, complex systems can be modeled simply, by the deep knowledge of the behavior of the real system, this will facilitate the control part. In addition, a special care should be taken when solving the (MI) coming from the Lyapunov analysis, this will have a huge impact on the desired performance of the observer.

For future work, our first step is to investigate the illogical behavior of the experimental estimation error before publishing a paper on the results of this Internship . Also, it's interesting to validate the observer on two phase flow. Further more, extending the approach to nonlinear hyperbolic systems for conservation laws, these laws are profiting as they govern the motion of many physical systems, which fall in our interest.

Appendix A

Model Implementation and Observer Design

A.1 Problem Formulation and Model Implementation: Chapter 2

A.1.1 Model Implementation

The equations of the discretized model are:
Hot fluid

$$\begin{cases} \frac{dh_i^H}{dt} = \frac{A_i^H \dot{m}_i^H (h_{i-1}^H - h_i^H)}{V^H(A_i^H \rho_i^H + B_i^H)} + \frac{\dot{m}_i^H - \dot{m}_{i+1}^H}{V^H(A_i^H \rho_i^H + B_i^H)} - \frac{A_i^H \pi D_1 dx \alpha (T_i^H - T_i^C)}{V^H(A_i^H \rho_i^H + B_i^H)} \\ \frac{dP_i^H}{dt} = \frac{\rho_i^H (\dot{m}_i^H - \dot{m}_{i+1}^H)}{V^H(A_i^H \rho_i^H + B_i^H)} - \frac{\dot{m}_i^H B_i^H (h_i^H - h_{i-1}^H)}{V^H(A_i^H \rho_i^H + B_i^H)} + \frac{B_i^H \pi D_1 dx \alpha (T_i^H - T_i^C)}{V^H(A_i^H \rho_i^H + B_i^H)} \\ \frac{d\dot{m}_i^H}{dt} = -(\frac{\dot{m}_{i+1}^{2,H}}{\rho_i^H} - \frac{\dot{m}_i^{2,H}}{\rho_{i-1}^H}) \frac{1}{A^H dx} + \frac{A^H (P_{i-1}^H - P_i^H)}{dx} - \frac{f_1 \dot{m}_H |\dot{m}_H|}{2 D_1 \rho_H A_H} \end{cases} \tag{A.1}$$

Cold fluid

$$\begin{cases} \frac{dh_i^C}{dt} = \frac{A_i^C \dot{m}_{i+1}^C (h_{i+1}^C - h_i^C)}{V^C(A_i^C \rho_i^C + B_i^C)} + \frac{\dot{m}_{i+1}^C - \dot{m}_i^C}{V^C(A_i^C \rho_i^C + B_i^C)} + \frac{A_i^C \pi D_1 dx \alpha (T_i^H - T_i^C)}{V^C(A_i^C \rho_i^C + B_i^C)} \\ \frac{dP_i^C}{dt} = \frac{\rho_i^C (\dot{m}_{i+1}^C - \dot{m}_i^C)}{V^C(A_i^C \rho_i^C + B_i^C)} - \frac{\dot{m}_{i+1}^C B_i^C (h_{i+1}^C - h_i^C)}{V^C(A_i^C \rho_i^C + B_i^C)} - \frac{B_i^C \pi D_1 dx \alpha (T_i^H - T_i^C)}{V^C(A_i^H \rho_i^C + B_i^C)} \\ \frac{d\dot{m}_i^C}{dt} = (\frac{\dot{m}_i^{2,C}}{\rho_{i+1}^C} - \frac{\dot{m}_{i-1}^{2,C}}{\rho_i^C}) \frac{1}{A^C dx} + \frac{A^C (P_{i+1}^C - P_i^C)}{dx} - \frac{f_1 \dot{m}_i^C |\dot{m}_i^C|}{2 D_H \rho^C A^C} \end{cases} \tag{A.2}$$

Where (for both fluid the same definition):
$A_i = \frac{\partial \rho_i}{\partial p}|_{h_i}$
$B_i = \frac{\partial \rho_i}{\partial h}|_{P_i}$
dx : width of the control volume
$V = A * dx$: volume of the control volume
$D_H = D_2 - D_1$: hydraulic Diameter

A.2 Observer Design: Chapter 3

A.2.1 Steady State Coefficients-Linear model

The nonlinear system (2.1)-(2.6) is linearized using first order Taylor expansion and we have the following matrices seen in chapter 3.

All the coefficients are computed at steady state:

$$A^S(x) = \begin{pmatrix} 0 & a_{12} & a_{13} & 0 & 0 & 0 \\ 1 & 0 & 0 & 0 & 0 & 0 \\ 0 & a_{32} & a_{33} & 0 & 0 & 0 \\ 0 & 0 & 0 & 0 & a_{45} & a_{46} \\ 0 & 0 & 0 & 1 & 0 & 0 \\ 0 & 0 & 0 & 0 & a_{65} & a_{66} \end{pmatrix}$$

$$a_{12} = A_H(\tfrac{\partial \rho}{\partial P}|_h)^H \qquad a_{13} = A_H(\tfrac{\partial \rho}{\partial h}|_P)^H$$

$$a_{32} = -A_H \qquad a_{33} = A_H\rho_H$$

$$a_{45} = A_C(\tfrac{\partial \rho}{\partial P}|_h)^C \qquad a_{46} = A_C(\tfrac{\partial \rho}{\partial h}|_P)^C$$

$$a_{65} = -A_C \qquad a_{66} = A_C\rho_C$$

$$B^S(x) = \begin{pmatrix} 1 & 0 & 0 & 0 & 0 & 0 \\ b_{21} & b_{22} & b_{23} & 0 & 0 & 0 \\ 0 & 0 & b_{33} & 0 & 0 & 0 \\ 0 & 0 & 0 & -1 & 0 & 0 \\ 0 & 0 & 0 & b_{54} & b_{55} & b_{56} \\ 0 & 0 & 0 & 0 & 0 & b_{66} \end{pmatrix}$$

$$b_{21} = \tfrac{2\dot{m}_H}{A_H\rho_H} \qquad b_{22} = A_H - \tfrac{\dot{m}_H^2(\frac{\partial \rho}{\partial P}|_h)^H}{A_H\rho_H^2}$$

$$b_{23} = -\tfrac{\dot{m}_H^2(\frac{\partial \rho}{\partial h}|_P)^H}{A_H\rho_H^2} \qquad b_{33} = \dot{m}_H$$

$$b_{54} = -\tfrac{2\dot{m}_C}{A_C\rho_C} \qquad b_{55} = -A_C + \tfrac{\dot{m}_C^2(\frac{\partial \rho}{\partial P}|_h)^C}{A_C\rho_C^2}$$

$$b_{56} = \tfrac{\dot{m}_C^2(\frac{\partial \rho}{\partial h}|_P)^C}{A_C\rho_C^2} \qquad b_{66} = -\dot{m}_C$$

$$C^S(x) = \begin{pmatrix} 0 & 0 & 0 & 0 & 0 & 0 \\ c_{21} & c_{22} & c_{23} & 0 & 0 & 0 \\ c_{31} & c_{32} & c_{33} & 0 & c_{35} & c_{36} \\ 0 & 0 & 0 & 0 & 0 & 0 \\ 0 & 0 & 0 & c_{54} & c_{55} & c_{56} \\ 0 & c_{62} & c_{63} & c_{64} & c_{65} & c_{66} \end{pmatrix}$$

- $c_{21} = f_1\frac{(2\dot{m}_H^2+\varepsilon)}{A_H\rho_H\sqrt{\dot{m}_H^2+\varepsilon}} - 2\frac{\dot{m}_H}{A_H\rho_H^2}$
- $c_{22} = -f_1\frac{\dot{m}_H\sqrt{\dot{m}_H^2+\varepsilon}(\frac{\partial \rho}{\partial P}|_h)^H}{A_H\rho_H^2} - \frac{\dot{m}_H^2(\frac{\partial \rho}{\partial P}|_h)_z^H}{A_H\rho_H^2} + 2\rho_{Hz}\dot{m}_H^2\frac{(\frac{\partial \rho}{\partial P}|_h)^H}{A_H\rho_H^3}$

- $c_{23} = -f_1 \frac{\dot{m}_H \sqrt{\dot{m}_H^2+\varepsilon} (\frac{\partial \rho}{\partial h}|_P)^H}{A_H \rho_H^2} - \frac{\dot{m}_H^2 (\frac{\partial \rho}{\partial h}|_P)_z^H}{A_H \rho_H^2} + 2\rho_{Hz} \dot{m}_H^2 \frac{(\frac{\partial \rho}{\partial h}|_P)^H}{A_H \rho_H^3}$
- $c_{31} = (\frac{dh}{dz})^H$
- $c_{32} = \alpha\pi D_1 (\frac{\partial T}{\partial P}|_h)^H = -c_{63}$
- $c_{33} = \alpha\pi D_1 (\frac{\partial T}{\partial h}|_P)^H = -c_{64}$
- $c_{35} = -\alpha\pi D_1 (\frac{\partial T}{\partial P}|_h)^C = -c_{65}$
- $c_{36} = -\alpha\pi D_1 (\frac{\partial T}{\partial h}|_P)^C = -c_{66}$
- $c_{54} = f_2 \frac{(2\dot{m}_C^2+\varepsilon)}{A_C \rho_C \sqrt{\dot{m}_C^2+\varepsilon}} + 2\frac{\dot{m}_C}{A_C \rho_C^2}$
- $c_{55} = -f_2 \frac{\dot{m}_C \sqrt{\dot{m}_C^2+\varepsilon} (\frac{\partial \rho}{\partial P}|_h)^C}{A_C \rho_C^2} + \frac{\dot{m}_C^2 (\frac{\partial \rho}{\partial P}|_h)_z^C}{A_C \rho_C^2} - 2\rho_{Cz} \dot{m}_C^2 \frac{(\frac{\partial \rho}{\partial P}|_h)^C}{A_C \rho_C^3}$
- $c_{56} = -f_2 \frac{\dot{m}_C \sqrt{\dot{m}_C^2+\varepsilon} (\frac{\partial \rho}{\partial h}|_P)^C}{A_C \rho_C^2} + \frac{\dot{m}_C^2 (\frac{\partial \rho}{\partial h}|_P)_z^C}{A_C \rho_C^2} - 2\rho_{Cz} \dot{m}_C^2 \frac{(\frac{\partial \rho}{\partial h}|_P)^C}{A_C \rho_C^3}$
- $c_{62} = -(\frac{dh}{dz})^C$

A.2.2 Global Exponential Stability : Proof

Taking the time derivative of (3.15) we have:

$$\begin{aligned}
\dot{V} &= \int_0^1 \partial_t \varepsilon^T |\Lambda|^{-1} Q(x) \varepsilon dx + \int_0^1 \varepsilon^T |\Lambda|^{-1} Q(x) \partial_t \varepsilon dx \\
&= \int_0^1 (\varepsilon^T F^T - \partial_x \varepsilon^T \Lambda^T) |\Lambda|^{-1} Q(x) \varepsilon dx + \int_0^1 \varepsilon^T |\Lambda|^{-1} Q(x) (F\varepsilon - \Lambda \partial_x \varepsilon) dx \\
&= \int_0^1 \varepsilon^T F^T |\Lambda|^{-1} Q(x) \varepsilon dx + \int_0^1 \varepsilon^T |\Lambda|^{-1} Q(x) F \varepsilon dx - \int_0^1 \partial_x \varepsilon^T \Lambda^T |\Lambda|^{-1} Q(x) \varepsilon + \varepsilon^T |\Lambda|^{-1} Q(x) \Lambda \partial_x \varepsilon dx
\end{aligned}$$

Noting that $|\Lambda|^{-1} Q(x) = Q(x) |\Lambda|^{-1}$ and $|\Lambda|^{-1} \Lambda = \check{I}_6 = diag[sign(\Lambda_i)]$, then

$$\dot{V} = \int_0^1 \varepsilon^T F^T |\Lambda|^{-1} Q(x) \varepsilon + \varepsilon^T |\Lambda|^{-1} Q(x) F \varepsilon dx - \int_0^1 \partial_x \varepsilon^T \check{I}_6 Q(x) \varepsilon + \varepsilon^T \check{I}_6 Q(x) \partial_x \varepsilon dx$$

Using the expansion: $\partial_x (\varepsilon^T \check{I}_6 Q(x) \varepsilon) = \partial_x \varepsilon^T \check{I}_6 Q(x) \varepsilon + \varepsilon^T \check{I}_6 Q(x) \partial_x \varepsilon + \varepsilon^T \overbrace{\check{I}_6 \partial_x (Q(x))}^{-2\mu Q(x)} \varepsilon$ implies that

$$\dot{V} = \underbrace{-[\varepsilon^T \check{I}_6 Q(x) \varepsilon]_0^1}_{\leq 0} + \int_0^1 (\underbrace{\varepsilon^T F^T |\Lambda|^{-1} Q(x) + |\Lambda|^{-1} Q(x) F - 2\mu Q(x)}_{\leq -2\gamma |\Lambda|^{-1} Q(x))}) \varepsilon dx$$

The constraints (3.16) and (3.17) guarantee that $\dot{V} \leq -2\gamma V$ and for $t \in R^+$ we have $V(\varepsilon(t,.) \leq e^{-2\gamma t} V(\varepsilon^0)$. To finalize the proof (3.15) implies that:

$$\lambda_{min} |\varepsilon|^2_{L^2((0,1);R^6)} \leq V(\varepsilon) \leq \lambda_{max} |\varepsilon|^2_{L^2((0,1);R^6)} \tag{A.3}$$

where $(\lambda_{min}, \lambda_{max})$ are the minimum and maximum Eigen values of the matrix $(|\Lambda|^{-1}Q(x))$ for all $x \in [0,1]$, respectively. We obtain the (GES) since:

$$\begin{aligned} \lambda_{min}|\varepsilon|^2_{L^2((0,1);R^6)} \leq e^{-2\gamma t}V(\varepsilon^0) \leq \lambda_{max}e^{-2\gamma t}|\varepsilon^0|^2_{L^2((0,1);R^6)} \\ \Leftrightarrow |\varepsilon|_{L^2((0,1);R^6)} \leq \sqrt{\frac{\lambda_{max}}{\lambda_{min}}}e^{-\gamma t}|\varepsilon^0|_{L^2((0,1);R^6)} \end{aligned} \tag{A.4}$$

which implies (3.14) and completes the proof.

References

[1] Serge Alinhac. *Hyperbolic partial differential equations*. Springer Science & Business Media, 2009.

[2] Peder Aursand et al. "Pipeline transport of CO 2 mixtures: Models for transient simulation". In: *International Journal of Greenhouse Gas Control* 15 (2013), pp. 174–185.

[3] Ian H. Bell et al. "Pure and Pseudo-pure Fluid Thermophysical Property Evaluation and the Open-Source Thermophysical Property Library CoolProp". In: *Industrial & Engineering Chemistry Research* 53.6 (2014), pp. 2498–2508. eprint: http://pubs.acs.org/doi/pdf/10.1021/ie4033999.

[4] S Brown et al. "Modelling the non-equilibrium two-phase flow during depressurisation of CO 2 pipelines". In: *International Journal of Greenhouse Gas Control* 30 (2014), pp. 9–18.

[5] Felipe Castillo et al. "Boundary observers for linear and quasi-linear hyperbolic systems with application to flow control". In: *Automatica* 49.11 (2013), pp. 3180–3188.

[6] Felipe Castillo et al. "Dynamic boundary stabilization of linear and quasi-linear hyperbolic systems". In: *Decision and Control (CDC), 2012 IEEE 51st Annual Conference on*. IEEE. 2012, pp. 2952–2957.

[7] Ababacar Diagne, Georges Bastin, and Jean-Michel Coron. "Lyapunov exponential stability of 1-D linear hyperbolic systems of balance laws". In: *Automatica* 48 (2012), pp. 109–114.

[8] M. K. Dobson. "Heat Transfer and Flow Regimes During Condensation in Horizontal Tubes". In: *PhD Thesis, University of Illinois* (1994).

[9] Tore Flåtten and Halvor Lund. "Relaxation two-phase flow models and the subcharacteristic condition". In: *Mathematical Models and Methods in Applied Sciences* 21.12 (2011), pp. 2379–2407.

[10] Volker Gnielinski. "New equations for heat and mass transfer in turbulent pipe and channel flow". In: *Int. Chem. Eng.* 16.2 (1976), pp. 359–368.

[11] Pierre-Olivier Lamare, Antoine Girard, and Christophe Prieur. "An optimisation approach for stability analysis and controller synthesis of linear hyperbolic systems". In: *ESAIM: Control, Optimisation and Calculus of Variations* 22.4 (2016), pp. 1236–1263.

[12] Daqian Li. *Controllability and observability for quasilinear hyperbolic systems*. American Institute of Mathematical Sciences Springfield, Ill, USA, 2010.

[13] Halvor Lund. "A hierarchy of relaxation models for two-phase flow". In: *SIAM Journal on Applied Mathematics* 72.6 (2012), pp. 1713–1741.

[14] Morin-Norwegian. "Mathematical modelling and numerical simulation of two phase multi-component flows of CO2 mixtures in pipes". In: *Thesis for the degree of Philosophiae Doctor,Trondheim. University of Science and Technology* (Oct. 2012).

[15] Svend Tollak Munkejord. "A numerical study of two-fluid models with pressure and velocity relaxation". In: *Adv. Appl. Math. Mech* 2 (2010), pp. 131–159.

[16] Michaël Ndjinga. "Influence of interfacial pressure on the hyperbolicity of the two-fluid model". In: *Comptes Rendus Mathematique* 344.6 (2007), pp. 407–412.

[17] Suhas Patankar. *Numerical heat transfer and fluid flow*. CRC press, 1980.

[18] GP Peterson. "An introduction to Heat pipes: Modeling". In: *Testing and Applications* (1994).

[19] Richard Saurel, Fabien Petitpas, and Rémi Abgrall. "Modelling phase transition in metastable liquids: application to cavitating and flashing flows". In: *Journal of Fluid Mechanics* 607 (2008), pp. 313–350.

[20] B Verlaat, M Van Beuzekom, and A Van Lysebetten. "CO2 cooling for HEP experiments". In: *Topical Workshop on Electronics for Particle Physics (TWEPP-2008), Naxos, Greece*. 2008, pp. 328–336.

[21] Atul Kumar Vij and WE Dunn. *Modeling of two-phase flows in horizontal tubes*. Tech. rep. Air Conditioning and Refrigeration Center. College of Engineering. University of Illinois at Urbana-Champaign., 1996.

[22] Cheng-Zhong Xu and Gauthier Sallet. "Exponential stability and transfer functions of processes governed by symmetric hyperbolic systems". In: *ESAIM: Control, Optimisation and Calculus of Variations* 7 (2002), pp. 421–442.

[23] Fairouz Zobiri, Emmanuel Witrant, and François Bonne. "PDE Observer Design for Counter-Current Heat Flows in a Heat-Exchanger". In: (2016).